This dissertation has been
microfilmed exactly as received

69-12,927

BANKS, Jr., Lawrence Edison, 1938-
THE MOTION OF BODIES THROUGH A VISCOUS MEDIUM.

The University of Oklahoma, Ph.D., 1969
Physics, general

University Microfilms, Inc., Ann Arbor, Michigan

Downloaded from SHAREOK. Persistent Handle URL: https://hdl.handle.net/11244/2547

THE UNIVERSITY OF OKLAHOMA

GRADUATE COLLEGE

THE MOTION OF BODIES THROUGH A VISCOUS MEDIUM

A DISSERTATION

SUBMITTED TO THE GRADUATE FACULTY

in partial fulfillment of the requirements for the

degree of

DOCTOR OF PHILOSOPHY

BY

LAWRENCE EDISON BANKS, JR.

Norman, Oklahoma

1969

THE MOTION OF BODIES THROUGH A VISCOUS MEDIUM

APPROVED BY

Sylvan J. Roerno

Jack Cohen

Arthur Bernhart

S. E. Babb, Jr.

Robert M. St. John

DISSERTATION COMMITTEE

ACKNOWLEDGEMENTS

There are many individual people and organizations that deserve recognition for their help in making possible the research summarized in these pages. The most important individual is Dr. Sybrand Broersma, who proposed the problem, supplied the necessary research apparatus from his National Science Foundation Research Grants, and directed the research.

I would also like to express my appreciation to Dr. R. T. Stevenson at Southwest Missouri State College, who urged me to return and complete my Ph.D. degree. Much of my work was dependent upon Dr. Broersma's former research assistants, mainly Bill Dodson. The apparatus used for the final part of this work was constructed by the highly skilled machinist, Mr. James Hood, who directs the Instrument Shop at the University of Oklahoma. Finally, there are the many teachers at the University of Oklahoma who are responsible for whatever knowledge of physics I may have.

The National Science Foundation has been kind enough to provide financial support by means of their Summer Grant for Graduate Research Assistants during the summer of 1963, and a Science Faculty Fellowship during the 12 month period which started in September, 1965. Finally, Southwest Missouri State College provided a one-half time leave of absence during the 1964 academic year. This institution also provided the time and necessary facilities during the summer of 1968 so that I could finish analyzing the experimental data, and write this dissertation.

TABLE OF CONTENTS

		Page
LIST OF TABLES		vi
LIST OF ILLUSTRATIONS		viii
Chapter		
I.	RESISTANCE OF FLUID MEDIA TO THE MOTION OF A SPHERE	1
	Introduction	1
	Motion of a Sphere in an Unbounded Medium	1
	Motion of a Sphere in a Cylindrical Container	2
	Motion of a Sphere when Line Singularities are Present.	3
II.	DEPENDENCE OF SPHERE DRAG ON REYNOLD'S NUMBER	11
	Experimental Apparatus	11
	Properties of the Viscous Medium	16
	Sphere Properties	22
	Determination of Fall Times	27
	Calculation of Uncorrected Viscosity	29
	Least-Mean-Square Fit of Raw Data	38
	Variations of Sphere Drag with Reynold's Number	39
	Conclusions	62
III.	EFFECT OF LINE BOUNDARIES ON SPHERE DRAG	64
	Experimental Apparatus	64
	Fall Time Determinations	66

TABLE OF CONTENTS (Cont'd.)

Chapter	Page
Variation of Sphere Drag with Number of Lines	84
Theoretical Analysis.	86
Conclusions	91
Appendix A	94
Appendix B	95
Bibliography	107

LIST OF TABLES

Table		Page
1.	Oil Density at Various Temperatures	21
2.	Sphere Parameters	28
3.	Uncorrected Viscosity for 1/8 PP Sphere	31
4.	Uncorrected Viscosity for 3/16 PP Sphere	32
5.	Uncorrected Viscosity for 3/32 N Sphere	33
6.	Uncorrected Viscosity for 1/4 PP Sphere	34
7.	Uncorrected Viscosity for 1/8 N Sphere	35
8.	Uncorrected Viscosity for 5/32 N Sphere	36
9.	Uncorrected Viscosity for 3/16 N Sphere	37
10.	Least-Mean-Square Fit of Uncorrected Viscosities to Equation (22)	40
11.	Comparison of η and η'(1/8 PP)	43
12.	Comparison of η and η'(3/16 PP)	44
13.	Comparison of η and η'(3/32 N)	45
14.	Comparison of η and η'(1/4 PP)	46
15.	Comparison of η and η'(1/8 N)	47
16.	Comparison of η and η'(5/32 N)	48
17.	Comparison of η and η'(3/16 N)	49
18.	Comparison of $\tilde{\eta}$(1/8 PP) and η'(3/16 PP)	54
19.	Comparison of $\tilde{\eta}$(1/8 PP) and η'(3/32 N)	55

LIST OF TABLES (Cont'd.)

Table		Page
20.	Comparison of $\tilde{n}$(1/8 PP) and n'(1/4PP)	56
21.	Comparison of $\tilde{n}$(1/8 PP) and n'(1/8 N)	57
22.	Comparison of $\tilde{n}$(1/8 PP) and $\tilde{n}$(5/32 N)	58
23.	Comparison of $\tilde{n}$(1/8 PP) and $\tilde{n}$(3/16 N)	59
24.	Horizontal Distance from Fall Line of Spheres to Line Boundaries	67
25.	One String Runs	74
26.	Two String Runs	76
27.	Four String Runs	78
28.	Six String Runs	80
29.	Twelve String Runs	81
30.	Best β_n Values from First Order Calculation	83
31.	Spherical Bodies	104
32.	Cylindrical Bodies	104

LIST OF ILLUSTRATIONS

Figure Page

1. Variation from Stokes' drag with Reynold's number, using η as the base 50

2. Variation from Stokes' drag with Reynold's number, using $\tilde{\eta}(1/8\ PP)$ as the base 60

3. Variation from Stokes' drag with Reynold's number 63

4. Variation in Sphere drag with String number 85

CHAPTER I

RESISTANCE OF FLUID MEDIA TO THE MOTION OF A SPHERE

Introduction

The purpose of the investigation to be summarized in these pages was two-fold. The first phase of the investigation dealt with a problem that has been considered many times in the past. That is, the variation of the correction to Stokes' law as a function of the Reynold's number. The second phase, on the other hand, dealt with a problem that, to this writer's knowledge, has never been treated before, either theoretically or experimentally. The problem dealt with the effect of line singularities in a fluid on the drag force experienced by a sphere moving parallel to the line.

The remainder of this chapter discusses the motivating interest of these problems to workers in fluid mechanics. Chapter II contains the experimental details and conclusions drawn from the first part of this investigation. Chapter III describes the second phase of the investigation, and the conclusions drawn from it. Finally, Appendix B summarizes several earlier investigations.

Motion of a Sphere in an Unbounded Medium

The development of the mathematical properties of the motion of fluids began as early as the time of Newton with his assumption that the

stress set up in a fluid as a result of its motion is directly proportional to the velocity gradient perpendicular to the fluid motion at the position of the stress.[1] In one dimension this assumption takes the mathematical form

$$f = \eta \frac{dv}{dx} \tag{1}$$

where the proportionality constant η is known as the coefficient of static viscosity, and is a measure of a particular fluid's resistance to shear. This assumption is easily verified by experiment.

The further development in the governing differential equation of fluid motion was culminated in 1823 with the development of the Navier-Stokes equation[2].

$$\rho\left\{\frac{\partial \vec{v}}{\partial t} + (\vec{v}\cdot\nabla)\vec{v}\right\} = \eta\nabla^2\vec{v} - \nabla p - \rho\nabla\phi + (\eta+\eta')\nabla(\nabla\cdot\vec{v}) \ , \tag{2}$$

where ρ is the fluid density, $\nabla\phi$ represents any conservative external force acting on the fluid, ∇p represents the force on the fluid resulting from pressure gradients, $\nabla^2\vec{v}$ is proportional to the force due to stress set up in the field, $d\vec{v}/dt$ is proportional to the time rate of change of momentum of a fluid element moving with the flow, and η' is an additional property of the fluid having to do with the internal forces set up by compression. This equation essentially represents momentum conservation at every point in the fluid. In all cases to be considered here, external forces will not be involved, and the fluid can be taken to be incompressible for all practical purposes. The equation then reduces to

$$\rho\left\{\frac{\partial \vec{v}}{\partial t} + (\vec{v}\cdot\nabla)\vec{v}\right\} = \eta\nabla^2\vec{v} - \nabla p \ , \qquad (3)$$

coupled with a condition of incompressibility given by

$$\nabla\cdot\vec{v} = 0 \ . \qquad (4)$$

Equations (3) and (4) are the governing differential equations for all flows to be considered here.

The general solution of this set of equations for the velocity field has never been obtained due to the nonlinearity of the term $(\vec{v}\cdot\nabla)\vec{v}$ which is proportional to the convective momentum of the fluid. The first approximate solution for a spherical body at rest in a highly viscous medium having a slow, uniform velocity at infinity was obtained by Stokes in 1853. With these conditions in mind, he ignored the time dependent and inertial effects, and solved the equations.

$$0 = \eta\nabla^2\vec{v} - \nabla p, \qquad \nabla\cdot\vec{v} = 0 \qquad (5)$$

subject to the boundary conditions at the sphere surface and at infinity. These equations have come to be known as Stokes' equations of steady, creeping motion. The end result of his calculation was the prediction of a drag force on the sphere due to the fluid of

$$\vec{D}_s = 6\pi\eta r\vec{U} \ , \qquad (6)$$

where r is the sphere radius and $\vec{U}$ is either the fluid velocity at infinity, or the negative of the sphere velocity in an otherwise quiescent fluid of infinite extent.

Since the initial solution by Stokes, there have been numerous attempts to improve his approximation, several of which are worth mentioning. In 1881, Whitehead tried a standard iteration technique of bringing the inertial effects into a second order solution by using the Stokes' field for the first order solution. However, his attempt failed since the resultant second order velocity field could not be made to satisfy the boundary condition at infinity[4]. In 1910, Oseen used the basic nondimensional parameter of the motion, known as Reynold's number and symbolized here by $Re \equiv \rho rU/\eta$, to argue that Stokes' solution was not even correct to first order since the inertial terms tended to dominate the flow at infinity. Based on this reasoning, he replaced the $(\vec{v}\cdot\nabla)\vec{v}$ terms by the linear terms $(\vec{U}\cdot\nabla)\vec{v}$, using the argument that the inertial effects were only important at very large distances from the body where the velocity field had a value very close to that at infinity. His solution for the resultant flow field lead to a prediction of the drag force on the sphere of[5]

$$\vec{D}_o = 6\pi\eta r\vec{U}(1 + \frac{3}{8}Re), \quad Re<<1 . \tag{7}$$

Even though the justification of this calculation left much to be desired, there was no improvement in its underlying assumptions until around 1955. At that time Kaplun and Lagerstrom suggested a division of the flow field into two regions: one near the body where an

iteration scheme like that proposed by Whithead would be used on the time-independent Navier-Stokes equations when expressed in coordinates suitable to that region, and one very far from the body where the Whitehead iteration scheme would be applied to the time independent Navier-Stokes equations when expressed in coordinate suitable to that region[6]. For obvious reasons the coordinates near the sphere have come to be known as Stokes' coordinates, while those far from the sphere have come to be known as Oseen coordinates. Then, since the resultant second order equations in either region can only be matched to either the inner or outer boundary, Kaplun proposed the existence of an overlap domain in which appropriate asymptotic expansions of the inner and outer region solutions could be matched to determine their remaining arbitrary constants. This technique falls under the general classification of singular perturbation problems[7,8].

In 1957, Proudman and Pearson used the Kaplun technique to solve the sphere problem. The end result of their calculation was that the sphere drag should be given by

$$\vec{D}_p = 6\pi\eta r\vec{U}[1 + \frac{3}{8}\,Re + \frac{9}{40}\,Re^2 \ell n Re + O(Re^2)], \quad Re<<1 , \qquad (8)$$

where the entrance of the ℓn Re term into the field is phenomenon now known as "switchback" and is an indirect result of the inertial terms[9-11]. Even though there exists no rigorous mathematical proof of the Kaplun technique, it is thought by many to be the best theoretical treatment available at this time, so that Eq. (8) should certainly be considered in the analysis of any experimental investigation in which the drag force on a sphere is measured.

It is fairly common knowledge that the experimental values of sphere drag often lie somewhere between the theoretical predictions of Stokes and Oseen, within the predicted accuracy of the experiment.[12] One notable exception is the recent work of Maxworthy who concludes that the Oseen prediction fits his data quite well for $0 < Re < 0.3$[13]. For several reasons it was decided that another try at this measurement was in order. First as has previously been stated, many earlier results are not in agreement with Maxworthy's conclusion.* It was also felt that the experimental accuracy reported by Maxworthy and others did not represent the limit in precision that could be obtained. Maxworthy's conclusion, based on only a few data points with the lowest value of Re being 0.2, was that the Oseen value was followed all the way to Re = 0; whereas, other workers, based in part on an analysis by Perry,[14] have come to the conclusion that the correction to Stokes' drag relation goes to zero for $Re \neq 0$. Furthermore, Broersma[15], Carrier[16], and others have concluded from their work that the correction to Stokes' law is definitely lower than that given by either Oseen or Proudman. Thus, it was felt that, with slightly more accurate measurements covering a more continous range of Re numbers, a better answer could be given concerning the variation in sphere drag with Reynold's number.

---

*See Figure 3, for a comparison of previous experimental lines with these found here.

Based on the discussion given above, the equation that should be used in an experimental investigation of this sort would be of the form

$$\vec{D} = 6\pi\eta r\vec{U}(1 + \alpha Re + \beta Re^2 \ell n\ Re + \gamma Re^2 + \ldots) \ , \qquad (9)$$

with α, β and γ serving as parameters to be determined by the experiment. However, the true experimental situation is more complicated than Eq. (9), since the body always moves in a finite rather than an infinite medium. Thus, it will be necessary to take this difference into account.

Motion of a Sphere in a Cylindrical Container

The actual experimental situation investigated here involved the motion of a small sphere in a large cylindrical container, with the ratio of sphere radius to container radius ranging from $\sim$ 0.004, for the smaller spheres to $\sim$0.007 for the larger spheres. Even though these ratios were quite small, they could not be ignored relative to inertial effects with Re $\sim$ 0.01. One further complication resulted from the necessary presence of the floor of the container. The ratio of the average sphere radius to the distance of the sphere from the container floor, when at the mid point of its fall, was found to be $\sim$0.005, which indicated that it could be ignored to first order for reasons to be explained below. Due to all these complications, it was felt best to restrict the experimental fit to first order corrections in Reynold's number and the boundaries.

The effect of the presence of more than one boundary symmetry on the motion of a sphere represents a very difficult theoretical problem.[17]

For a sphere moving axially in an infinitely long cylinder, several theoreticians have shown that Stokes' law should be multiplied by the first order correction factor[18-20]

$$1/(1 - 2.10\ r/L), \tag{10}$$

where L represents the container radius. On the other hand, it has been shown that a sphere moving perpendicular to an infinite plane wall in an otherwise unbounded fluid results in an alteration of Stokes' law by the multiplicative factor[21]

$$(1 + 9/8 \cdot r/B), \tag{11}$$

where B represents the average distance from the sphere center to the wall.

However, it is not correct to combine the correction factors given by Eqs. (10) and (11) independently either from a theoretical or experimental standpoint, since the resultant correction factor is far too high[22]. The appropriate correction to Stokes' law for a finite cylindrical container has been extensively studied by Tanner[23]. The effect of the floor of the container is strongly dependent upon the ratio of B to L. His calculations and experimental results show that for $B/L \sim 1.32$, as it was in this experiment, the appropriate correction for the container floor is $\sim 1 \times 10^{-4}$ a/B which, when coupled with the a/B values here, gives a negligible first order effect.

Based on these considerations the equation that has been used in the analysis here is given by

$$\vec{D} = 6\pi\eta r\vec{U}(1 + \alpha Re)(1 + 2.10\ r/L) \ . \qquad (12)$$

Actually, until now each bracketed factor has only been proven in absence of the other. In this thesis it is shown that the effect of inertia and of the wall are related. Tucker and Broersma[24] considered the case of exact stationarity and found $\alpha = 0$.

Motion of a Sphere When Line Singularities are Present

In any situation involving the slow, steady motion of a sphere through a viscous fluid, there are always one or more boundaries at some finite distance from the sphere. There have been numerous theoretical and experimental investigations of the effect of various boundaries on the drag force experienced by a sphere. An extremely comprehensive compliation of these investigations is given in the recent treatise by Happel and Brenner.[25]

However, the particular problem of a sphere moving in the vicinity of one or more line singularities that are parallel to the direction of motion of the sphere, appears not to have been treated. Such an analysis should be of importance for at least two reasons. First, there should be an intrinsic interest in measuring the drag increase on the sphere when moving in this fashion, and, for one singularity at least, it should be possible to calculate this effect directly. Furthermore, as the number of such singularities is increased, it might be possible to gain some insight into the manner in which the effect of various boundary symmetries is built up. Thus, the manner in which a cylindrical boundary is built up has been considered in some detail in Chapter III.

Based on the general form of boundary corrections that have been calculated, the experimental data in this case was assumed to obey a relation of the form

$$D = 6\pi\eta aU(1 + \alpha Re)(1 + \beta_n \, r/s) \, , \tag{13}$$

where n is an integer representing the number of line singularities present at distance s from the sphere center, and β_n is the numerical factor to be determined from the experimental results. The effects of the other boundaries were ignored in Eq. (13) since in all cases r/s was more than an order of magnitude larger than r/L and r/B.

CHAPTER II

DEPENDENCE OF SPHERE DRAG ON REYNOLD'S NUMBER

Experimental Apparatus

The Fluid Container and Cathetometer

The container for the viscous medium in this investigation is a large metal tank having cylindrical symmetry. Its height is 105 cm and its diameter is 78 cm. It has a plexiglass window in one side of it that was used for viewing, and its top is partially covered with a metal flange for heat shielding. The tank was placed in a large sand-box both for leveling and thermal insulation. Previous to this investigation the tank had been coated on the inside with several layers of oil resistant white epoxy. Since the spheres used in these experiments were white, a final coat of oil resistant black epoxy was painted over the white in such a manner that two thin white lines were left directly behind the upper and lower portions of the plexiglass window. Then two strips of black plastic tape were placed on the outside of the window in close alignment with the white lines on the inside of the tank.

Two microscopes were mounted on a cathetometer so that each level in the tank could be viewed from a distance. The distance between the two sets of reference lines was determined with this cathetometer, after it had been placed in the exact position where the fall-

time measurements were to be taken, and carefully leveled. The microscopes were focused on a three meter rod placed along the axis of the tank, and their position was adjusted to give a reproducible arrangement for deciding when the leading edge of a falling sphere was aligned with the tank reference lines and the cathetometer crosshairs. The final setting decided upon was such that the distance over which the spheres were timed was 34.500 ± 0.005 cm.

Container Placement

From prior knowledge of the strongly temperature dependent properties of the viscous medium, it was known that the tank and its immediate surroundings would have to be maintained at an almost constant temperature, if the accuracy desired was to be obtained For this reason the container was placed in a well-insulated room, and all measurements were taken through a double plexiglass window by means of the cathetometer arrangement described above, viewed from the outside laboratory.

As a check on the temperature at a given point in the room, a Beckman thermometer, capable of showing temperature differences of 0.01°C, was mounted on a stand between the tank and an outside window. This temperature was constantly monitored both before and during the experimental runs. In most cases the temperature in the room was found to be constant to 0 01°C provided the laboratory room temperature was not undergoing rapid fluctuations. Runs were never made if this thermometer showed temperature variations as large as 0.02°C. Due to the thermal insulation between the outside of the tank and the center of the tank, where the spheres actually fell, this precaution should have been more than sufficient.

Temperature Measurement

Two thermometers, which had previously been subjected to a relative calibration when placed together, were ~~placed~~ on the outside of the tank at the upper and lower reference marks. Insulation was placed over these thermometers so that a check could be maintained on any temperature gradients in the container. Even when the Beckman thermometer showed no measurable temperature fluctuation in the room, these thermometers showed a constant temperature differential of $0 < \Delta T \leq 0.10^{\circ}$ C with the lower temperature occurring at the lower reference line.

The difference in height between the reference lines corresponded to a pressure difference in the medium of approximately 0.06 atm. Using an approximate figure for the compressibility of the medium gives an estimated density difference at these levels of $\sim 2 \times 10^{-5} \mathrm{gm/cm^3}$, which is slightly less than the accuracy with which the oil density could be measured. This estimate was found to be in close agreement with the variation in oil density as a function of temperature (discussed later), since according to those measurements $\Delta T < 0.10^{\circ}$ C would imply $\Delta\rho < 4 \times 10^{-5} \mathrm{gm/cm^3}$. Thus, comparison of the data obtained here with theoretical predictions based on an incompressible fluid should be meaningful.

The temperature used in all calculations later was obtained from a standard thermometer that was suspended over the tank in such a way that it could be lowered into the center of the tank from out-

side the room. In all cases temperature readings on this thermometer were taken when it was located at the approximate midpoint of the distance over which the sphere fell. The smallest separation of the etched lines on this thermometer corresponded to a temperature difference of 0.05° C; however, when viewing it with the cathetometer, it was possible to estimate visually to the nearest 0.02° C.

An experimental arrangement such as the one described above does have the disadvantage that the container temperature cannot be controlled. However, the temperature will naturally vary slowly so that measurements can be taken at many different temperatures over a period of time. Furthermore, there might be a definite advantage of this equilibrium arrangement over one in which the temperature is controlled. As noted above, the equlibrium state of the medium is apparently one in which a small temperature gradient exists. Thus, if the temperature of the medium is "forced", by means of a surrounding water bath say, to maintain an almost constant temperature throughout, it is quite possible that local instabilities might occur resulting in convective mixing. To this writer's knowledge there is no proof that such mixing will actually occur; however, if it does, the fall times of a sphere might not be as reproducible as those found with an arrangement such as the one described here.

Lighting

The lighting of the tank was accomplished by means of a 15 watt, water-cooled, fluorescent lamp that was mounted just over the top of the tank. This light was only kept on during the actual fall time of the spheres, and it was possible to adjust the water flow rate so that significant changes in the Beckman thermometer were not caused by its presence. The additional precaution was taken of measuring the midpoint temperature of the oil bath before and after each run.

Sphere Dropping Mechanism

Since it was necessary to keep the container isolated to the extent noted above, a mechanism was necessary for dropping the spheres by remote control. To accomplish this task, a plexiglass disk was constructed having a single hole. This disk was mounted horizontally so that the hole was directly over a vertical tube through which the spheres ultimately entered the oil. Another plexiglass disk having twelve holes was then mounted directly over the first disk in such a way that it could be turned about its vertical axis by a small motor wired to a switch outside the room. In this way 12 or more spheres could be placed on this apparatus in a planned arrangement 24 hours before the actual run was to be made. By running the motor for a precalculated time interval each of the holes in the top disk could then be brought, in turn, into alignment with the vertical tube.

The actual entry of a sphere into the oil was made by means of a tube of diameter slightly larger than that of the sphere. This tube extended into the oil for several inches, and served three purposes. First of all, it served to bring the sphere into a state of motion that resulted in a very smooth entry into the large container. Next, it had previously been found that almost all the air bubbles, that tend to form on the sphere when it first enters the oil, will break away from the sphere before it leaves the tube. The tube was not an unqualified success in this respect, since several runs had to be thrown out due to air bubbles on the sphere; however, in most runs the sphere was evidently free of air bubbles. Finally, the close ratio of the tube diameter to the sphere diameter served to align the sphere very close to the axis of the tube. This close alignment was essential to the measurements that were made in the second phase of this investigation. A small basket was placed on the container floor to catch the spheres. This basket was raised by nylon cords having heavy hooks attached to one end. These cords were never present during an actual experimental run.

Properties of the Viscous Medium

The oil chosen for these experiments is a very clear oil known as Whiterex 334. Its viscosity had previously been measured with a #300 Cannon viscometer and a #400 Eubank-Fisher viscometer both of which had been commercially calibrated relative to standard oils. A least-mean-square fit of these values to a line of the form

$$\ell n\ \eta = \ell n \eta_o + \lambda T \qquad (14)$$

gives

$$\ell n \eta_o = 0.693 \quad ,$$

$$\lambda = - 0.074 \ ,$$

over a temperature range from 20.00° C. The standard deviation in the η values found from the above line is given by

$$\sigma(\eta) = 0.01 \ .$$

The data points did not fit the above line this well outside the temperature range indicated above; however, this temperature range did cover the range over which fall-time measurements were taken.

Determination of Oil Density

Pycnometer Calibration

In order to determine the density of the oil as a function of temperature, the standard pycnometer technique was used. To insure sufficient accuracy in these measurements, a water bath was used that was capable of maintaining a constant temperature to ±0.015° C. Since the accuracy of these measurements is crucial to the final results, it is perhaps of some interest to describe the details.

Initially, the pycnometer was thoroughly cleaned, and placed in a drying oven. Upon its removal from the drying oven, it was immediately placed in a freshly prepared dessicator, and was left there until it was in thermal equilibrium with the room in which a Sartorius balance was located. Its mass was then determined on this balance to $\pm 2 \times 10^{-4}$gm.

The pycnometer was next rinsed and very slowly filled with distilled, deionized water that had previously been heated to remove all air bubbles. At the time of filling the pycnometer, the water temperature was slightly below room temperature. The filled pycnometer was then lowered almost up to its top in the constant temperature bath until equilibrium with the bath temperature, which was slightly above room temperature, was attained. At this point, while the pycnometer was still in the bath, the water bead at the top of the pycnometer, which had formed due to the slightly increased temperature, was carefully removed with the tip of a tissue, so that the pycnometer was exactly filled at the known bath temperature. The pycnometer was then removed from the bath, and a clean glass slide was placed on its top. Then the remaining outside surface was carefully cleaned with a highly volitile solvent and dried with tissues. Finally, the pycnometer was transferred, using tissue so that finger dirt would not adhere to it, to the balance where its mass was determined.

Based on these measurements, the volume of the pycnometer was determined in the following manner:

$$M(\text{pycnometer dry}) = 54.1584 \text{ gm.}$$

$$M(\text{pycnometer and water}) = 156.2505 \text{ gm at } T = 28.90^\circ \text{ C}$$

$$\rho(\text{water at } T = 28.90^\circ\text{C}) = 0.99570 \text{ gm/cm}^3$$

$$\rho(\text{air}) = 1.174 \times 10^{-5} \text{ gm/cm}^3*$$

$$\rho(\text{balance weights}) = 8.4 \text{ gm/cm}^3*$$

$\therefore$,

$$M(\text{pycnometer in vacuo}) = M(\text{in air}) \left[1 + \rho(\text{air})\left(\frac{1}{\rho(H_2O)} - \frac{1}{\rho(\text{weights})}\right)\right]$$

$$= 1.00119\ M(\text{in air}) ,$$

and so

$$V(\text{pycnometer}) = \frac{156.2505 - 54.1584}{0.99570}\ (1.00119)$$

$$= 102.6550 \text{ cm}^3 .$$

Measurement of oil density.

For the determination of the mass of the pycnometer when filled with the oil to be used in the experiment, the same procedure as that described above for the pycnometer when filled with water was used. It should be noted that by starting the determinations at a temperature below the median temperature for which the oil density is desired, it is a simple matter to continue to increase the bath temperature in small increments and simply wipe off the resultant oil bead on the top, without ever needing to refill the pycnometer.

---

*These figures were supplied as nominal values by the manufacturer of the balance, with the guarantee of $\pm 2 \times 10^{-4}$ gm on the instrument used here.

Cooling the pycnometer and oil more than about 6° C below room temperature is quite another matter, since water then tends to condense on the outside and may even get inside. Also, after the pycnometer has been removed from a bath whose temperature is lower than that of the room, the oil will immediately begin to expand. Thus, one must be quite careful not to wipe off the oil that comes out of the top of the pycnometer after its removal from the bath. Finally, for a small increase in the bath temperature that is still below room temperature for the next measurement, it is usually necessary to refill the pycnometer.

Subjecting the resultant values of ρ_o, T to a least-mean-square fit to the line

$$\rho_o = \bar{\rho}_o + \varepsilon T \tag{16}$$

gives*

$$\bar{\rho}_o = 0.88732 \text{ gm/cm}^3,$$

$$\varepsilon = 0.000411 \text{ gm/C° cm}^3.$$

The associated standard deviations are

$$\sigma(\bar{\rho}_o) = 0.00001 \text{ gm/cm}^3$$

$$\sigma(|\varepsilon|) = 0.000005 \text{ gm/C° cm}^3$$

$$\sigma(\rho_o) = 0.00003 \text{ gm/cm}^3$$

provided those points lying $2\sigma(\rho_o)$ or more from the line are discarded. The data points used for the above determination are given in Table 1,

---

*All numerical calculations in this paper were carried out on an Ollivetti-Underwood Programmar 101. Thus, in order to minimize machine error, no attempt was made to round off intermediate numerical results. In all cases the associated standard deviations of numerical results are given, so that the proper number of significant figures is clear.

Table 1. Oil density at various temperatures.

T(°C)	M(pycn. + oil in air)(gm)	ρ_o(gm/cm^3)
18.01	146.2160	0.88002
19.00	146.1668	0.87954
20.00	146.1216	0.87910
20.50	146.1011	0.87890
20.62	146.0960	0.87885
21.46	146.0591	0.87849
22.32	146.0242	0.87815
23.00	145.9945	0.87786
24.00	145.9935	0.87746
24.70	145.9238	0.87717
26.20	145.8581	0.87653
27.10	145.8171	0.87613

where ρ_o in each case has been found from the relation

$$\rho_o(\text{oil}) = \frac{[M(\text{pycn. + oil}) - 55.9849]}{102.6550} (1.00119)\,\text{gm/cm}^3.$$

The mass 55.9849 gm in the above relation corresponds to the mass of the empty pycnometer plus a wire holder attached to it for this set of measurements. As a final note, the effect of the volume coefficient of expansion of the pyrex glass in the pycnometer has been ignored here. The worst error in ρ_o due to this effect occurred in the measurement at 18.01° C, since the volume of the pycnometer was determined at 28.90° C. Using the numbers from Table 1 and a volume coefficient of expansion for pyrex of 1×10^{-5} $\text{cm}^3/\text{C}°$, gives the associated error in ρ_o to be 1×10^{-6} gm/cm^3.

Sphere Properties

Choice of Spheres

In order to investigate the variation of sphere drag with Re number in the first phase of this investigation, and the effect of line boundaries on sphere drag in the second phase, it was found necessary to use spheres of varying density and size. Also, since a good part of the experiment depended upon having motions with $Re \ll 1$, the sphere densities had to be rather close to that of the oil. It was finally decided that spheres of 4 different plastics would be used. The plastic types were polypropylene, polyethylene, nylon and teflon. However, upon receipt of the polyethylene and the teflon spheres, it was found that they were not even close to the specified sphericity tolerance; therefore, they were not used in the actual experiments.

For the polypropylene spheres, the following nominal diameter sizes were used: 1/8", 3/16" and 1/4". For the nylon spheres, the nominal diameters used were: 3/32", 1/8", 5/32" and 3/16". These densities and sizes permitted motions with Reynold's number varying from $\sim$0.006 to $\sim$0.260 over a fairly continuous range.

Determination of Sphere Density

Since it is quite possible for plastic materials to absorb some of the fluid with which they are in contact, the precautionary step of "soaking" each of the spheres for a period of about one week was taken.* After this period the sphere parameters were determined. These parameters were then checked at the conclusion of the experimental runs.

The driving force used in the experiments was that of gravity so that it was the difference between the sphere density and oil density that was ultimately used in the calculations. Thus, it was decided that the sphere density should be measured directly using the pycnometer technique according to the procedure discussed below. In this way the necessary accuracy in the density difference was obtained.

---

*In the manufacturer's specification of the nylon sphere properties, the surface penetration of water in a 24 hour period was given as 1/8 the sphere thickness or $\sim$1.5 per cent of its volume; for polypropylene the surface penetration was only 0.01 per cent of its volume for water.

By mixing two infinitely soluble fluids, one of density less than that of a particular sphere and the other of density greater than that of the sphere, it was possible to achieve a fluid state in which the gravitational force on the sphere was almost exactly balanced by the buoyant force on it due to the fluid mixture. Then the density of the resultant mixture was determined using a technique very much like that described for the oil density measurements.

In order to get some idea of the final drift velocity of the sphere that had to be obtained for the accuracy desired, consider the relation that holds for $Re \equiv \rho Ur/\eta << 1$, namely

$$6\pi\eta rU(1 + \alpha Re)/(1 - 2.1\ r/L) = \frac{4}{3}\pi r^3 \Delta\tilde{\rho} g,$$

where $\Delta\tilde{\rho} \equiv \rho(\text{sphere}) - \rho(\text{fluid mixture})$. In all cases considered in this set of measurements Re was small enough to be ignored. Clearly, the necessary variable measure of the condition $\Delta\tilde{\rho} \to 0$ is given by the magnitude of U. Thus, the working relation given above should be put in the form

$$U = \frac{2r^2 g}{9\eta}(1 - 2.1\ r/L)\Delta\tilde{\rho}.$$

Since the oil density was known to $0(10^{-5}\text{gm/cm}^3)$, it was necessary to achieve a fluid mixture in which the final drift velocity, in conjunction with the other parameters given in the relation above, would make $\Delta\tilde{\rho} < \sim 0(10^{-5}\text{gm/cm}^3)$. In the fluid mixture used the cgs unit magnitudes were $\eta \sim 10^{-3}$, $r^2 \sim 4\text{x}10^{-2}$, $g \sim 10^3$ and $r/L < \sim 10^{-1}$. Inserting these approximate figures into the working relation gives

$$U \sim 0.5 \text{ cm/min.} \qquad (17)$$

The final U values ultimately attained in the actual measurements were at least an order of magnitude smaller than the above figure.

Before discussing the actual fluid mixtures used for the two plastic types, one difference in the experimental technique from that used in measuring the oil density should be pointed out. Initially, once the balance of the sphere in the fluid mixture had been attained, in a position as close to the middle of the mixture as possible due to slight density gradients that arose as the mixture sat, the mixture was transferred to the pycnometer and immediately weighed. However, the resultant densities were not reproducible with the same accuracy that had previously been attained for the oil density, namely $\pm 3 \times 10^{-5} gm/cm^3$.

The desired accuracy was finally achieved by first transferring the filled pycnometer, with the sphere in it, to the water bath. Then the bath temperature was adjusted until the desired U-balance was achieved. At that point the fluid mixture was leveled at the top of the pycnometer, and the usual procedure was followed for determining its mass.*

The fluid mixture used for determining the nylon sphere densities was obtained by mixing distilled water with a saturated solution of potassium iodine. The sphere buoyancy was observed to be

---

*The pycnometer was initially filled so that a small bead of the fluid mixture remained on its top in case the final desired temperature was slightly below room temperature. Also, evaporation had to be carefully guarded against.

quite sensitive to the addition of alternate drops of these two fluids, and the only procedural difficulty encountered was that of making sure there were no residual air bubbles on the sphere when balanced.

The fluid mixture used for the polypropylene spheres was obtained by mixing distilled water and propyl-alcohol. This alcohol was used since its boiling point of 97.5° C was a very close match to that of water. In any case the beakers containing the fluid mixtures for both plastic types were kept sealed as much as possible.

The densities found in the manner described above are listed in Table 2.

Determination of Sphere Radius

The other sphere parameter that is necessary for the final calculations is the radius. This parameter was initially measured with a measuring microscope with an accuracy of $\pm 5 \times 10^{-4}$cm. However, various diameters of the spheres were found to vary by as much as 1×10^{-3}cm so that an averaging process was necessary. Furthermore, it is r^2 that actually enters into the calculations so that the residual error of 1×10^{-3}cm present in the direct r measurements was definitely too large.

Thus, it was decided that the average value of r would be used which follows quite simply from weighing the spheres on a very accurate balance, and using the relation

$$\langle r \rangle = \left(\frac{3m}{4\pi\rho} \right)^{1/3}, \qquad (18)$$

where ρ was known from the direct density determinations already made. For spheres 3/16 PP, 1/4 PP, 5/32 N, 3/16 N a Sartorius balance was used that had a precision of $\pm 2 \times 10^{-5}$gm. For spheres 1/8 PP, 3/32 N and 1/8 N, a Kahn electrobalance, having a precision in this range of 5×10^{-6}gm, was used. Combining these results according to the relation given for $\langle r \rangle$ above gives an average value that is correct to $\pm 1.0 \times 10^{-5}$cm. The results of these measurements are listed in Table 2.

Determination of Fall Times

A total of 60 different experimental runs were made, each of which involved the timing of at least 12 different spheres. However, several of these times were thrown out due to the presence of one or more tiny air bubbles on the spheres as has been previously mentioned. These bubbles were easily detected by looking through the cathetometer telescopes, and were almost always very near the top of the sphere, so that the observer was able to rule out most such occurrences automatically.

After the first several runs, it was found that the occurrence of air bubbles on the spheres could be reduced by coating the spheres with a thin layer of oil as they were placed in the sphere dropping mechanism. With the spheres coated in this fashion, they tended to adhere to the sides of the vertical fall tube. To counteract this effect a probe was mounted over this tube in such a way that it could be lowered into the tube, from outside the room, to free the sphere.

Table 2. Sphere Parameters.

Sphere type	mass (mg)	ρ (gm/cm^3)	<r> (cm)
1/8 PP	15.568	0.90766	0.15998
3/16 PP	49.70	0.90573	0.23573
3/32 N	8.072	1.16584	0.11824
1/4 PP	119.23	0.90611	0.31550
1/8 N	18.927	1.16584	0.15708
5/32 N	37.28	1.16593	0.19690
3/16 N	64.44	1.16594	0.23630

In order to insure that the spheres fell into an otherwise undisturbed fluid in each case, a definite time interval was allowed to elapse between each fall. The lower limit of this time in each case was determined from an appropriate two-sphere interaction formula.[26] These times found to be less than 5 to 10 minutes after the end of the preceding run, in order to insure that the two-sphere interaction was more than an order of magnitude smaller than the accuracy desired.

Calculation of Uncorrected Viscosity

Since the true viscosity of the oil was only known from direct measurements to ±0.1, it was decided to first calculate a value for the oil viscosity that had not been corrected for inertial or boundary effects. This parameter of the motion, sybmolized here by η' is given according to Stokes' law by

$$\eta' = \frac{2r^2 g\Delta\rho}{9U} \, .$$

When the parameters that have been measured are placed in the above relation, it takes the form

$$\eta' = \left(\frac{2\langle r\rangle^2 g}{9\ell} \right)\left(\overline{\Delta\rho} \pm |\varepsilon|T\right)t \, ,$$

where $\overline{\Delta\rho} \equiv \rho(\text{sphere}) - \bar{\rho}_o$, $\ell \equiv$ distance over which the spheres fell and t is the time taken for the sphere to fall thorugh this distance. All times were measured with a Gallet stopwatch. The observer calibrated himself and the watch to WWV with an accuracy of ±0.05 sec for

the time intervals of order 50 sec and larger. The accuracy achieved in the actual measurements for time intervals of order 20 sec was probably no better than ±0.1 sec due to stop and start reactions of the observer; however, this effect should have been fairly random.

An estimate of the accuracy of η' to be expected from these measurements can be obtained quite simply. From Eq. (19) it follows that

$$|\varepsilon(\eta')| = \left[\frac{4r|\varepsilon(r)|gt}{9\ell} + \frac{2r^2g|\varepsilon(\ell)|}{9\ell^2} t + \frac{2r^2g|\varepsilon(t)|}{9\ell} \right] (\overline{\Delta\rho} + |\varepsilon|T)$$

$$+ \frac{2r^2gt}{9\ell} \left[|\varepsilon(\overline{\Delta\rho})| + |\varepsilon(|\varepsilon|t)| \right] .$$

The cgs unit magnitudes typical to these parameters are $r \sim 10^{-1}$, $g \sim 10^{3}$, $t \sim 10^{2}$, $\ell \sim 3x10$, $\overline{\Delta\rho} \sim 10^{-2}$ and $|\varepsilon|T \sim 10^{-2}$. The errors associated with them are $\varepsilon(r) \sim 1x10^{-5}$, $\varepsilon(t) \sim 5x10^{-2}$, $\varepsilon(\ell) \sim 10^{-2}$, $\varepsilon(\overline{\Delta\rho}) \sim 6x10^{-5}$, and $\varepsilon(|\varepsilon|T) \sim 1x10^{-4}$. Thus,

$$|\varepsilon(\eta')| \sim 8x10^{-6} + 5x10^{-6} + 3x10^{-5} + 5x10^{-4} + 3x10^{-4} \sim 1x10^{-3}.$$

Clearly, the limiting factor in the measurements is the result of the errors present in the sphere and oil density.

The above analysis explains why it was necessary to push the pycnometer technique, used for the density measurements, to the limit. Evidently, the only way to decrease the error limit from that found above would be to use denser spheres, of smaller radius to maintain low Re values, and a fluid medium with much less temperature dependence on its parameters.

The values of η' found for each of the spheres are listed below in Tables 3, 4, 5, 6, 7, 8, and 9.

Table 3. Uncorrected viscosity for 1/8 PP sphere.

T	t_{exp}	η'	$\ell n \eta'$
19.85	440.81	2.0295	0.7078
20.10	431.29	1.9928	0.6895
20.35	422.00	1.9569	0.6713
20.52	416.16	1.9345	0.6598
20.57	414.06	1.9261	0.6555
20.60	412.78	1.9210	0.6528
20.62	412.23	1.9190	0.6518
21 00	400.09	1.8725	0.6273
21.05	398.17	1.8640	0.6232
21.25	390.52	1.8342	0.6066
21.40	385.85	1.8161	0.5967
21.45	383.38	1.8058	0.5910
21.80	372.64	1.7639	0.5675
21.90	370.00	1.7538	0.5618
22.25	357.40	1.7024	0.5320
22.70	344.02	1.6489	0.5001
23.00	355.50	1.6148	0.4792
23.45	321.57	1.5573	0.4430
23.55	319.53	1.5496	0.4380

Table 4. Uncorrected viscosity for 3/16 PP sphere

T	t_{exp}	η'	$\ell n \eta'$
19.85	218.90	2.0400	0.7129
20.00	216.07	2.0183	0.7022
20.10	214.32	2.0050	0.6956
20.20	212.38	1.9899	0.6881
20.40	208.57	1.9602	0.6730
20.52	206.32	1.9426	0.6640
20.57	205.85	1.9397	0.6625
20.60	205.24	1.9348	0.6600
20.62	205.10	1.9341	0.6596
20.70	203.20	1.9185	0.6515
20.80	201.72	1.9075	0.6458
21.00	198.04	1.8784	0.6304
21.10	196.84	1.8693	0.6258
21.25	193.59	1.8432	0.6115
21.40	190.93	1.8220	0.5999
21.50	189.38	1.8099	0.5933
21.55	188.67	1.8045	0.5902
21.60	187.56	1.7952	0.5851
21.83	184.00	1.7672	0.5694
22.30	177.22	1.7141	0.5389
22.70	170.71	1.6610	0.5074
23.00	166.09	1.6232	0.4844
23.40	161.02	1.5830	0.4593
23.45	160.43	1.5783	0.4563
23.55	159.09	1.5674	0.4494
23.65	158.50	1.5639	0.4472
24.50	148.60	1.4844	0.3950

Table 5. Uncorrected viscosity for 3/32 N sphere

T	t_{exp}	η'	ℓnη'
19.85	80.41	2.0343	0.7101
20.00	79.23	2.0049	0.6956
20.10	78.75	1.9930	0.6896
20.20	78.18	1.9789	0.6825
20.40	77.20	1.9546	0.6702
20.50	76.57	1.9390	0.6621
20.57	76.23	1.9306	0.6578
20.61	75.90	1.9223	0.6535
21.00	73.88	1.8722	0.6271
21.25	72.60	1.8404	0.6100
21.40	71.89	1.8228	0.6004
21.45	71.62	1.8161	0.5967
21.50	71.28	1.8076	0 5920
21.83	69.58	1.7653	0.5683
22.05	68.45	1.7372	0.5532
22.25	67.57	1.7153	0.5396
22.30	67.34	1.7096	0.5363
22.40	66.85	1.6974	0.5291
22.70	65.30	1.6588	0.5061
23.00	63.76	1.6204	0.4826
23.45	61.64	1.5675	0.4495
23.55	61.06	1.5530	0.4401
23.65	60.54	1.5400	0.4317

Table 6. Uncorrected Viscosity for 1/4 PP sphere

T	t_{exp}	n'	ℓnn'
19.85	121.48	2.0569	0.7212
20.00	120.04	2.0372	0.7116
20.10	118.88	2.0206	0.7034
20.20	117.71	2.0037	0.6950
20.40	116.21	1.9842	0.6852
20.52	115.18	1,9702	0.6781
20.57	114.77	1.9647	0.6753
20.62	114.49	1.9613	0.6736
20.70	113.45	1.9459	0.6657
20.80	112.44	1.9314	0.6582
21.00	110.61	1.9057	0.6448
21.05	110.06	1.8977	0.6406
21.25	108.03	1.8682	0.6250
21.40	106.70	1.8494	0.6148
21.45	106.13	1.8409	0.6102
21.50	105.80	1.8365	0.6078
21.55	105.40	1.8309	0.6048
21.83	102.88	1.7946	0.5848
22.20	99.41	1.7436	0.5559
22.70	95.38	1.6852	0.5219
23.00	92.77	1.6463	0.4985
23.45	89.13	1.5920	0.4650
23.55	88.20	1.5777	0.4559
23.65	87.50	1.5674	0.449472

Table 7. Uncorrected viscosity for 1/8 N sphere.

T	t_{exp}	η'	$\ell n \eta'$
19.85	45.69	2.0401	0.7130
20.00	45.18	2.0177	0.7019
20.10	44.76	1.9992	0.6927
20.40	44.11	1.9711	0.6785
20.50	43.86	1.9602	0.6730
20.52	43.87	1.9589	0.6724
20.57	43.67	1.9519	0.6688
20.60	43.56	1.9470	0.6663
20.62	43.50	1.9444	0.6649
20.80	43.00	1.9226	0.6536
20.94	42.66	1.9077	0.6459
21.00	42.36	1.8945	0.6389
21.10	42.10	1.8831	0.6329
21.25	41.42	1.8562	0.6185
21.40	41.06	1.8374	0.6083
21.45	40.93	1.8317	0.6052
21.50	40.81	1.8265	0.6024
21.80	40.08	1.7946	0.5847
21.83	40.02	1.7920	0.5833
22.30	38.34	1.7179	0.5411
22.70	37.30	1.6722	0.5141
23.00	36.48	1.6407	0.4951
23.15	36.18	1.6231	0.4843
23.45	35.40	1.5888	0.4629
23.55	35.17	1.5787	0.4566
23.65	34.91	1.5672	0.4493

Table 8. Uncorrected viscosity for 5/32 N sphere.

T	t_{exp}	η'	$\ell n\ \eta'$
19.85	29.64	2.0801	0.7324
20.62	28.03	1.9693	0.6776
21.43	26.50	1.8639	0.6226
21.45	26.47	1.8760	0.6291
22.20	25.18	1.7731	0.5727
22.30	25.00	1.7606	0.5656
23.00	23.66	1.6679	0.5116
23.65	22.42	1.5820	0.4754

Table 9. Uncorrected viscosity for 3/16 N sphere.

T	t_{exp}	η'	$\ell n\ \eta'$
20.20	20.43	2.0661	0.7256
21.00	19.48	1.9722	0.6791
21.25	19.20	1.9446	0.6650
21.40	18.98	1.9227	0.6537
21.50	18.90	1.9149	0.6496
22.20	18.20	1.8458	0.6129
23.00	17.10	1.7362	0.5517
23.55	16.59	1.6858	0.5222

Least-Mean-Square Fit of Raw Data

It is a well-established fact that many liquids have a normal curve given by[27]

$$\ell n\, \eta = A_\eta + E_\eta / k\, T_{ab} \,, \tag{20}$$

where A_η and E_η are adjustable parameters. However, it is a simple matter to show that

$$\ell n\, \eta = \ell n\, \eta_o - \lambda (T_c - 20^\circ\, C), \tag{21}$$

where $\ell n\, \eta_o$ and λ are now the adjustable parameters, is equivalent to the original normal curve provided the temperature range is small. In the data found above, the temperature range is 4° C so that the lines given by Eqs. (20) and (21) will be equivalent to $0(10^{-4})$ in $\ell n\, \eta$.

In all cases the raw data was subjected to a least-mean-square fit to one or more lines of the form given by Eq. (21). This equation was found to be visually preferable in eliminating bad points because of the smaller slope associated with it, and was quite sufficient to determine the associated "viscosity" to $0(10^{-3})$. In several cases points were thrown out since they lay more than 2σ away from the line. In two cases, 1/4 PP and 1/8 N, it was clear that a single line was not sufficient to cover the entire temperature range; therefore, the slope and intercept of two lines of the form given by Eq. (21) were determined for these two cases.

The results of these least-mean-square fits to a line of the form

$$\ell n\ \eta' = \ell n\ \eta_o' - \lambda' T, \qquad (22)$$

where the primes serve to indicate that the parameters have yet to be corrected for wall and inertial effects, are shown in Table 10.

Variations of Sphere Drag with Reynold's Number

General

Once the best values of the parameters associated with line given by Eq. (22) have been determined, it is possible to inquire about the variation of the sphere drag with Reynold's number. The values of η' which have now been determined are related to the true viscosity η by

$$\eta' = \eta(1 + \alpha Re)/(1 - 2.10\ r/L), \qquad (23)$$

where, as usual, it is assumed that the effects of the outer boundary and inertia are independent to first order.

Defining

$$\tilde{\eta} \equiv \eta'(1 - 2.10\ r/L)\ , \qquad (24)$$

it holds that

$$\frac{\tilde{\eta}}{\eta} - 1 = \alpha Re\ , \qquad (25)$$

but clearly this last relation is equivalent to normalizing the wall corrected drag D_W with respect to the Stokes' drag D_S, since also

Table 10. Least-mean-square fit of uncorrected viscosities to Equation (22).

Sphere Type	T-Range(°C)	$\ell n \eta'_o$	$\lambda'(°C^{-1})$	$\sigma(\ell n \eta'_o)$	$\sigma(\lambda')$	$\sigma(\ell n \eta)$
1/8 PP	19.85 - 23.65	0.6972	0.0727	0.0004	0.0003	0.0009
3/16 PP	19.85 - 23.65	0.7027	0.0724	0.0004	0.0003	0.0012
3/32 N	19.85 - 23.00	0.6975	0.0704	0.0007	0.0004	0.0015
1/4 PP	20.00 - 23.65	0.7162	0.0727	0.0006	0.0003	0.0015
1/4 PP	19.85 - 21.00	0.7128	0.0675	0.0010	0.0014	0.0013
1/4 PP	20.52 - 23.65	0.7174	0.0733	0.0004	0.0002	0.0008
1/8 N	19.85 - 23.65	0.7074	0.0705	0.0008	0.0004	0.0022
1/8 N	19.85 - 20.62	0.7030	0.0606	0.0004	0.0008	0.0006
1/8 N	20.50 - 23.65	0.7094	0.0713	0.0004	0.0002	0.0008
5/32 N	19.85 - 23.65	0.7206	0.0673	0.0009	0.0005	0.0013
3/16 N	20.20 - 23.55	0.7397	0.0610	0.0011	0.0006	0.0015

$$\frac{D_w}{D_s} - 1 = \alpha Re \qquad (26)$$

Thus, by plotting $\tilde{\eta}/\eta - 1$ versus Re it should be possible to answer several questions concerning the variations of the correction to Stokes' drag with Re: 1) Does the drag correction approach zero as Re approaches zero? 2) If the answer to the first question is in the affirmative, is this approach only in the limit Re = 0; or, is Stokes' law applicable to finite Re values? 3) What is the <u>average</u> value of the parameter α as $Re \to 0$?

The concept of an average value of α in the last question is essential. Even though only first order corrections are being considered at this point, it is well-known that higher order terms in Re must be present. Hence, α may well change over certain ranges in Re. In plotting αRe versus Re, the slope of the curve is given by

$$\frac{d(\alpha Re)}{dRe} = \alpha + Re \frac{d\alpha}{dRe} \equiv \langle\alpha\rangle \quad , \qquad (27)$$

where $\langle\alpha\rangle$ will be a meaningful number for a given Re range only if $\alpha >> Re(d\alpha/dRe)$ over that range.

A serious difficulty presents itself at this point due to the fact that the true viscosity of the fluid is only known to $0(10^{-2})$, so that the error in αRe due to the inaccuracy in this parameter is given by

$$\begin{aligned} \varepsilon(\alpha Re) &= \varepsilon\left(\frac{\tilde{\eta}'}{\eta} - 1\right) \\ &= \frac{\tilde{\eta}'}{\eta^2}\ \varepsilon(\eta) \\ &\sim 0.007 \end{aligned}$$

An error of this size is larger than some αRe values that will be found for the 1/8 PP sphere.

η Base

In any case, it is still of interest to look at the resultant plot of αRe vs. Re using the directly measured values of η, provided the associated error limits are kept in mind. Thus, Tables 11, 12, 13, 14, 15, 16 and 17 list the values of η', η', αRe, Re and α for each of the spheres at several temperature values in the range covered by the experiment.

The manner in which the Reynold's number has been calculated in these tables should be mentioned. Since, by definition,

$$\mathrm{Re} \equiv \frac{\rho r U}{\eta} = \frac{\rho r \ell}{\eta t} , \tag{28}$$

it is necessary to find the proper t-value that should go into this relation for a given sphere at a given temperature. In all fairness to the spirit of the comparison being made here, this t-value should be that associated with the sphere when falling in an infinite medium. So take

$$t = \frac{9\tilde{\eta}'\ell}{2r^2\Delta\rho} ,$$

which gives Re to be

$$\mathrm{Re} = \frac{2r^3 g}{9} \frac{(\overline{\Delta\rho} + |\varepsilon|T)(\bar{\rho}_o - |\varepsilon|T)}{\tilde{\eta}\,\eta} \tag{29}$$

A simple error analysis shows that the values of Re found in this fashion will be correct within 1.5×10^{-4}.

Table 11. Comparison of η and η'(1/8 PP).

T-20	η	η'	$\tilde{\eta}$*	αRe	Re	α**
0	2.000	2.0082	1.9905	-0.0047	0.0056	-0.838
0.5	1.927	1.9365	1.9195	-0.0038	0.0060	-0.638
1.0	1.857	1.8673	1.8590	-0.0032	0.0066	-0.494
1.5	1.789	1.8006	1.7848	-0.0023	0.0071	-0.328
2.0	1.724	1.7364	1.7211	-0.0016	0.0077	-0.214
2.5	1.661	1.6743	1.6596	-0.0008	0.0084	-0.097
3.0	1.601	1.6145	1.6003	-0.0004	0.0091	-0.045

*Wall correction: $\tilde{\eta} = \eta'(1 - 2.10\ r/L) = \eta'(0.9912)$.

**$\alpha = 1/\mathrm{Re}\left(\frac{\tilde{\eta}}{\eta} - 1\right)$.

Table 12. Comparison of η and η'(3/16 PP).

T--20	η	η'	$\tilde{\eta}$*	αRe	Re	α
0	2.000	2.0193	1.9930	-0.0034	0.0167	-0.206
0.5	1.927	1.9474	1.9220	-0.0025	0.0181	-0.140
1.0	1.857	1.8780	1.8536	-0.0018	0.0197	-0.091
1.5	1.789	1.8112	1.7876	-0.0074	0.0213	-0.034
2.0	1.724	1.7468	1.7240	0.0000	0.0231	0.002
2.5	1.661	1.6845	1.6626	0.0009	0.0250	0.039
3.0	1.601	1.6246	1.6035	0.0015	0.0271	0.057

*Wall correction: $\tilde{\eta} = \eta(0.9870)$.

Table 13. Comparison of η and η'(3/32 N)

T-20	η	η'	$\tilde{\eta}$*	αRe	Re	α
0	2.000	2.0087	1.9959	-0.0021	0.0227	-0.095
0.5	1.927	1.9392	1.9266	-0.0002	0.0244	-0.010
1.0	1.857	1.8720	1.8598	0.0015	0.0263	0.060
1.5	1.789	1.8072	1.7954	0.0034	0.0282	0.121
2.0	1.724	1.7446	1.7333	0.0053	0.0304	0.175
2.5	1.661	1.6841	1.6732	0.0071	0.0327	0.217
3.0	1.601	1.6258	1.6153	0.0090	0.0352	0.257

*Wall correction: $\tilde{\eta} = \eta'(0.9935)$.

Table 14. Comparison of η and η'(1/4 PP).

T-20	η	η'	$\bar{\eta}$*	αRe	Re	α
0	2.000	2.0372	2.0018	0.0009	0.0403	0.022
0.5	1.927	1.9684	1.9341	0.0037	0.0437	0.084
1.0	1.857	1.9000	1.8670	0.0053	0.0474	0.113
1.5	1.789	1.8340	1.8021	0.0073	0.0514	0.142
2.0	1.724	1.7695	1.7387	0.0085	0.0557	0.153
2.5	1.661	1.7062	1.6765	0.0093	0.0604	0.154
3.0	1.601	1.6463	1.6176	0.0104	0.0655	0.158

*Wall correction: $\bar{\eta} = \eta'(0.9826)$.

Table 15. Comparison of η and $\eta'(1/8\ N)$.

T-20	η	η'	$\tilde{\eta}$*	αRe	Re	α
0	2.000	2.0296	2.0120	0.0060	0.0528	0.113
0.5	1.927	1.9602	1.9431	0.0083	0.0568	0.146
1.0	1.857	1.8914	1.8750	0.0097	0.0611	0.159
1.5	1.789	1.8259	1.8101	0.0116	0.0657	0.176
2.0	1.724	1.7627	1.7474	0.0135	010707	0.191
2.5	1.661	1.7016	1.6869	0.0153	0.0761	0.201
3.0	1.601	1.6427	1.6285	0.0173	0.0818	0.211

*Wall correction: $\tilde{\eta} = \eta'(0.9913)$

Table 16. Comparison of η and η'(5/32 N).

T-20	η	η'	$\tilde{\eta}$*	αRe	Re	α
0	2.000	2.0556	2.0332	0.0166	0.1030	0.161
0.5	1.927	1.9876	1.9659	0.0186	0.1105	0.168
1.0	1.857	1.9217	1.9007	0.0219	0.1186	0.184
1.5	1.789	1.8581	1.8378	0.0267	0.1276	0.209
2.0	1.724	1.7965	1.7769	0.0331	0.1374	0.241
2.5	1.661	1.7371	1.7182	0.0350	0.1473	0.238
3.0	1.601	1.6795	1.6612	0.0383	0.1581	0.242

*Wall correction: $\tilde{\eta} = \eta'(0.9891)$.

Table 17. Comparison of η and $\eta'(3/16\ N)$.

T-20	η	η'	$\tilde{\eta}^*$	αRe	Re	α
0	2.000	2.09549	2.06824	0.03412	0.17517	0.1948
0.5	1.927	2.03256	2.00613	0.03945	0.18723	0.2107
1.0	1.857	1.97140	1.94578	0.04612	0.20039	0.2302
1.5	1.789	1.91223	1.88737	0.05440	0.21480	0.2533
2.0	1.724	1.85473	1.83061	0.06431	0.23057	0.2789
2.5	1.661	1.79899	1.77561	0.06964	0.24641	0.2826
3.0	1.601	1.74503	1.72234	0.07646	0.26370	0.2900

*Wall correction: $\tilde{\eta} = \eta'(0.9870)$.

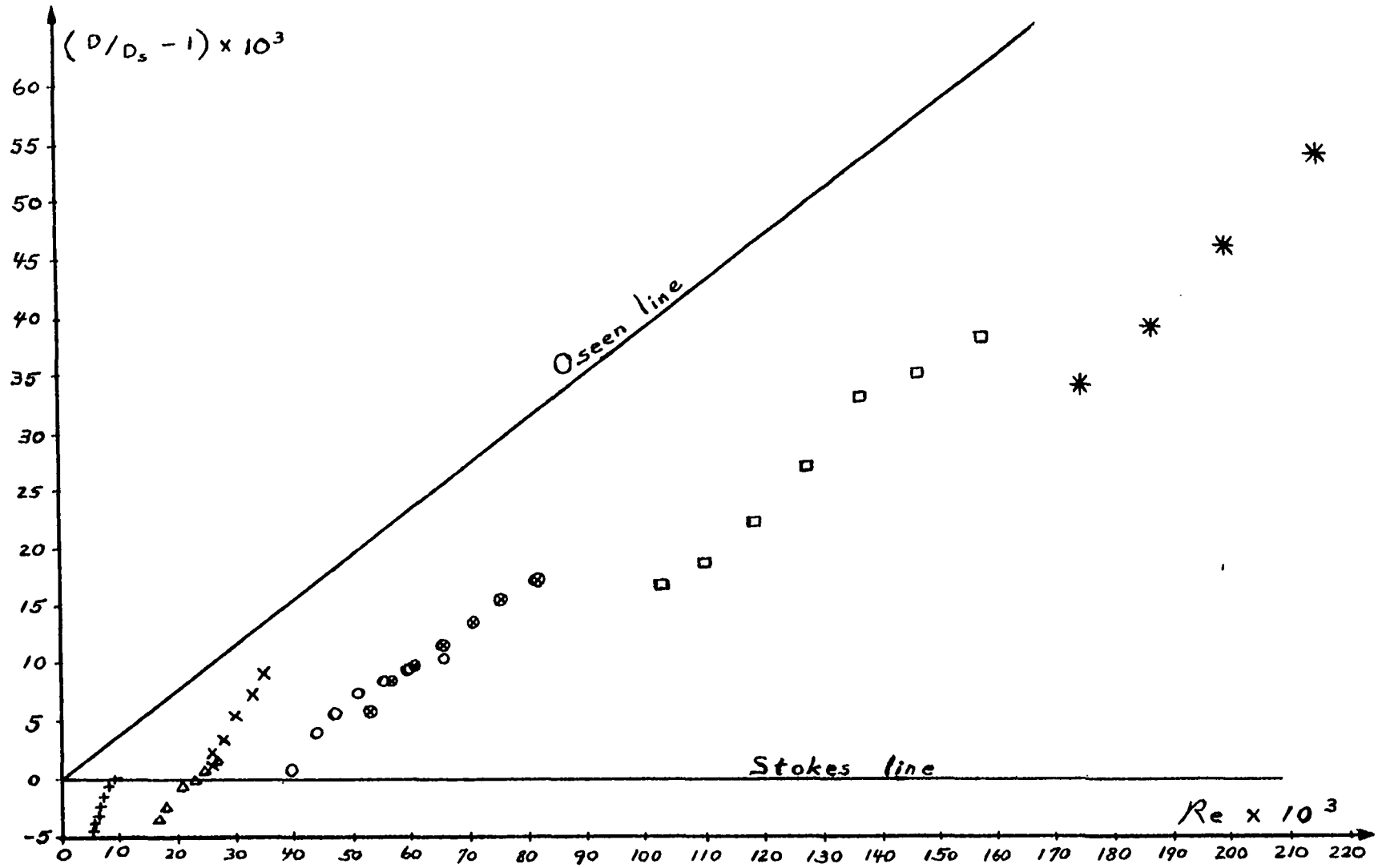


Figure 1. Variation from Stokes' drag with Reynold's number, using η as the base.
Legend: + ++ 1/8 PP sphere, Δ Δ Δ 5/16 PP sphere, x xx 3/32 N sphere, o o o 1/4 PP sphere, ⊗ ⊗ ⊗ 1/8 N sphere
□ □ □ 5/32 N sphere, * * * 3/16 N sphere.

When a plot of these values is made (Fig. 1), several interesting features appear. First, the points for the various spheres are not well connected. In fact, all the values of α Re associated with the 1/8 PP sphere are negative; whereas, several of the αRe values associated with the 3/16 PP sphere and the 3/32 N sphere are also negative. Looking at the average value of αRe associated with each of the spheres, it would definitely appear that α decreases as Re decreases in the range 0.01 Re 0.035, to the extent that Stokes' law lies within the error limits for Re 0.03.

Furthermore, it would appear that these average values assume a fairly constant slope for Re>0.04. When the αRe values for Re>0.04 are subjected to a least-mean-square fit to the line

$$\alpha Re = \langle\alpha\rangle Re + (\alpha Re)_o \quad , \tag{30}$$

where $\langle\alpha\rangle$ and $(\alpha Re)_o$ are, respectively, the slope and intercept of the line, it is found that

$$\langle\alpha\rangle = 0.244,$$

$$(\alpha Re)_o = -0.003.$$

The standard deviations associated with these values are given by

$$\sigma\{(\alpha Re)_o\} = 0.0013$$

$$\sigma(\langle\alpha\rangle) = 0.0133$$

$$\sigma(\alpha Re) = 0.003.$$

Clearly $\varepsilon\{(\alpha Re)_o\}$ and $\varepsilon(\alpha Re)$ must still be taken to be ~ 0.007 due to the absolute error present in the calculation.

Assuming that negative values of αRe are highly unlikely, it may be asserted that the αRe values associated with the 1/8 PP sphere must be positive. Then the error limit of 0.007 associated with the η values must be no greater than ~ 0.002 at Re ~ 0.006. A somewhat smaller positive value is found if it is assumed that $<\alpha>$ found above retains any significance in this region, since at Re ~ 0.006,

$$<\alpha> Re \sim (0.244)(0.006) \sim 0.0015.$$

η(1/8 PP) Base

In any case it is evidently meaningful to take $\tilde{\eta}(1/8PP)$ as a base for the other spheres, under the assumption that the 1/8 PP sphere will have αRe-values of order 0 ± 0.002. The error associated with the αRe-values for the other spheres is then

$$\varepsilon(\alpha Re) = \frac{\varepsilon\,\tilde{\eta}}{\tilde{\eta}(1/8)}\,[1 + \alpha(1/8)Re(1/8)] + \frac{\tilde{\eta}\;\varepsilon\,\tilde{\eta}(1/8)}{[\tilde{\eta}(1/8)]^2}\,[1+ \alpha(1/8)Re(1/8)]$$

$$+ \frac{\tilde{\eta}}{\tilde{\eta}(1/8)}\,\varepsilon[\alpha(1/8)Re(1/8)]$$

$$\sim 0.0007 + 0.0007 + 0.002$$

$$\sim 0.0034\ ,$$

which is only half the error that was present when the η values were used.

With this comparison in mind, Tables 18, 19, 20, 21, 22 and 23 list the values of η', $\bar{\eta}'$, αRe, Re and α for each of the remaining spheres at several of the temperature values in the range covered by the experiment. The relation used for determining the Re values in these tables is

$$Re = \frac{2\ r^3 g}{9} \frac{(\Delta\bar{\rho} + |\varepsilon|T)(\bar{\rho}_o - |\varepsilon|T)}{\eta'\ \bar{\eta}(1/8\ PP)} \tag{31}$$

Due to the improved accuracy of $\bar{\eta}(1/8\ PP)$ over the original η values, the error in these values of Re is given by $<\sim 0.00005$.

Table 18. Comparison of $\tilde{\eta}$(1/8 PP) and η'(3/16 PP)

T-20	$\tilde{\eta}$(1/8PP)	η'	$\tilde{\eta}$	αRe	Re	α
0	1.99059	2.0193	1.9930	0.00124	0.0168	0.073
0.5	1.91951	1.9474	1.9220	0.00134	0.0182	0.073
1.0	1.85092	1.8780	1.8536	0.00147	0.0197	0.074
1.5	1.78480	1.8112	1.7876	0.00161	0.0214	0.075
2.0	1.72114	1.7468	1.7240	0.00171	0.0231	0.073
2.5	1.65964	1.6845	1.6626	0.00180	0.0251	0.072
3.0	1.60035	1.6246	1.6035	0.00197	0.0271	0.072

Table 19. Comparison of $\tilde{\eta}$(1/8 PP) and η'(3/32 N)

T-20	$\tilde{\eta}$(1/8PP)	η'	$\tilde{\eta}$	αRe	Re	α
0	1.99059	2.0087	1.9956	0.00256	0.0228	0.121
0.5	1.91951	1.9392	1.9266	0.00369	0.0245	0.150
1.0	1.85092	1.8720	1.8598	0.00481	0.0263	0.182
1.5	1.78480	1.8072	1.7954	0.00596	0.0283	0.210
2.0	1.72114	1.7446	1.7333	0.00706	0.0304	0.231
2.5	1.65964	1.6841	1.6732	0.00817	0.0327	0.249
3.0	1.60035	1.6258	1.6153	0.00934	0.0352	0.265

Table 20. Comparison of $\tilde{\eta}$(1/8 PP) and η'(1/4 PP)

T-20	$\tilde{\eta}$(1/8PP)	η'	$\tilde{\eta}$	αRe	Re	α
0	1.99059	2.03725	2.00180	0.00563	0.04057	0.1388
0.5	1.91951	1.96840	1.93415	0.00763	0.04395	0.1736
1.0	1.85092	1.90007	1.86701	0.00869	0.04761	0.1825
1.5	1.78480	1.83406	1.80215	0.00972	0.05157	0.1885
2.0	1.72114	1.76954	1.73875	0.01023	0.05587	0.1831
2.5	1.65964	1.70624	1.67655	0.01019	0.06051	0.1684
3.0	1.60035	1.64630	1.61765	0.01081	0.06554	0.1649

Table 21. Comparison of $\tilde{\eta}$(1/8 PP) and η'(1/8 N)

T-20	$\tilde{\eta}$(1/8PP)	η'	$\tilde{\eta}$	αRe	Re	α
0	1.99059	2.0296	2.0120	0.0107	0.0531	0.202
0.5	1.91951	1.9592	1.9431	0.0123	0.0571	0.215
1.0	1.85092	1.8914	1.8750	0.0130	0.0613	0.212
1.5	1.78480	1.8259	1.8101	0.0141	0.0659	0.215
2.0	1.72114	1.7627	1.7474	0.0153	0.0708	0.215
2.5	1.65964	1.7016	1.6869	0.0164	0.0761	0.215
3.0	1.60035	1.6427	1.6285	0.0175	0.0818	0.214

Table 22. Comparison of $\tilde{\eta}$(1/8PP) and $\tilde{\eta}$(5/32 N)

T-20	$\tilde{\eta}$(1/8PP)	η'	$\tilde{\eta}$	αRe	Re	α
0	1.99059	2.0556	2.0332	0.0214	0.1030	0.207
0.5	1.91951	1.9876	1.9659	0.0241	0.1105	0.218
1.0	1.85092	1.9217	1.9007	0.0264	0.1186	0.227
1.5	1.78480	1.8581	1.8378	0.0297	0.1276	0.232
2.0	1.72114	1.7965	1.7769	0.0324	0.1374	0.236
2.5	1.69564	1.7371	1.7182	0.0353	0.1473	0.239
3.0	1.60035	1.6795	1.6612	0.0380	0.1581	0.240

Table 23. Comparison of $\tilde{\eta}$(1/8 PP) and $\tilde{\eta}$(3/16 N)

T-20	$\tilde{\eta}$(1/8PP)	η'	$\tilde{\eta}$	αRe	Re	α
0	1.99059	2.0954	2.0682	0.0390	0.1760	0.221
0.5	1.91951	2.0325	2.0061	0.0451	0.1882	0.239
1.0	1.85092	1.9714	1.9457	0.0512	0.2013	0.254
1.5	1.78480	0.9122	1.8873	0.0574	0.2154	0.266
2.0	1.72114	1.8547	1.8306	0.0636	0.2304	0.276
2.5	1.69564	1.7989	1.7756	0.0698	0.2464	0.283
3.0	1.60035	1.7450	1.7223	0.0762	0.2636	0.289

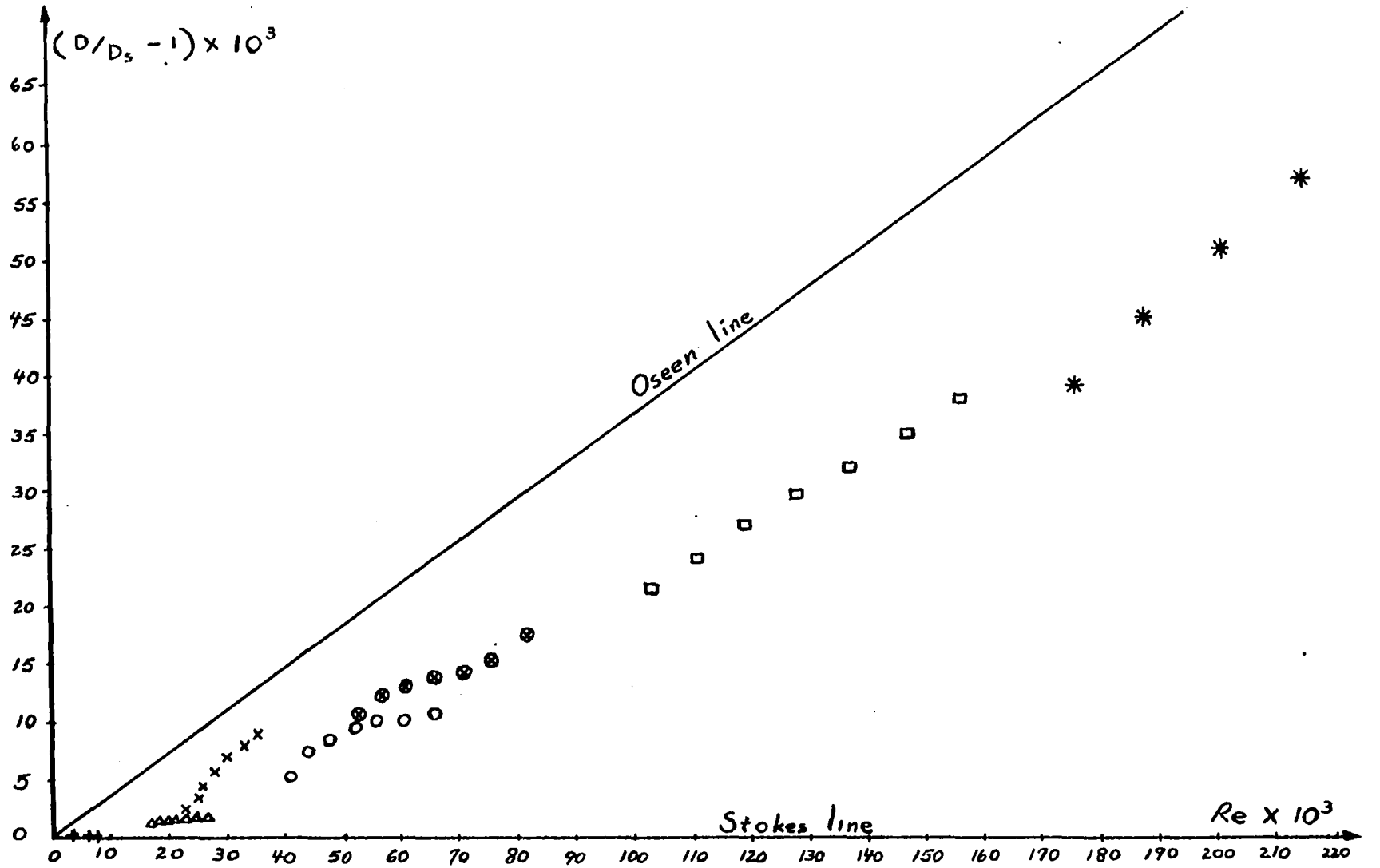


Figure 2. Variation from Stokes drag with Reynolds number, using $\tilde{\eta}$(1/8PP) as the base.
Legend: +++ 1/8 PP sphere, ΔΔΔ 3/16 PP sphere, XXX 3/32 N sphere, o oo 1/4 PP sphere, ⊗⊗⊗ 1/8 N sphere, □ □ □ 5/32 N sphere, * * * 3/16 N sphere.

The graph that results in this case (Fig. 2) shows a much improved correlation between the various spheres, while retaining several general features of the original graph. A general accelerated decrease in the value of αRe is observed for $Re < 0.030$ whereas, the slope maintains a fairly constant value for $0.030 < Re < 0.180$. Thus, the values in this range have again been submitted to a least-mean-square fit to a line of the form

$$\alpha Re = \langle\alpha\rangle Re + (\alpha Re)_o \quad . \tag{30}$$

The results of this fit are

$$\langle\alpha\rangle = 0.225,$$

$$(\alpha Re)_o = 0.0003,$$

with associated standard deviations of

$$\sigma(\langle\alpha\rangle) = 0.006,$$

$$\sigma\{(\alpha Re)_o\} = 0.0005,$$

$$\sigma(\alpha Re) = 0.001 \quad .$$

Here again, we must take $\varepsilon\{(\alpha Re)_o\}$ and $\varepsilon(\alpha Re)$ to be ~ 0.0034 due to the errors associated with the parameters used in the calculations.

Conclusions

In summary, both plots of αRe versus Re appear to show that $\alpha \sim 0$ for $Re < 0.009$. There is a sharp increase in α over the range $0.015<Re<0.030$; whereas, α achieves a fairly constant value over the range $0.035<Re<0.175$ giving a good value for $<\alpha>$. Finally, there appears to be another sharp increase in α from $0.175<Re<0.260$. Fig. 3 compares the two lines found here to several other well-known theoretical and experimental investigations. It would appear that the present investigation is most in accord with the experimental work of Castelman[28] and Broersma[29]; whereas, none of the accepted theoretical lines fit the data very well. The only exception to this last statement occurs in the range $Re \leq 0.02$ where Stokes' law appears to be far superior to any of the others. This conclusion is in close accord with Carrier.[30]

The experimental results discussed above cannot be denied, since they are more precise than any given previously. On the basis of these results, there is no doubt that the most commonly quoted correction to Stokes' law, namely 3/8 Re, is not correct. The Kaplun technique evidently does give the best possible solution to the Navier - Stokes' equations for $Re<<1$; however, the solution simply does not explain what happens in a tank. Thus, it may well be that the Navier - Stokes' solutions are simply not valid for fluids for $0< Re<<1$, in a finite container.

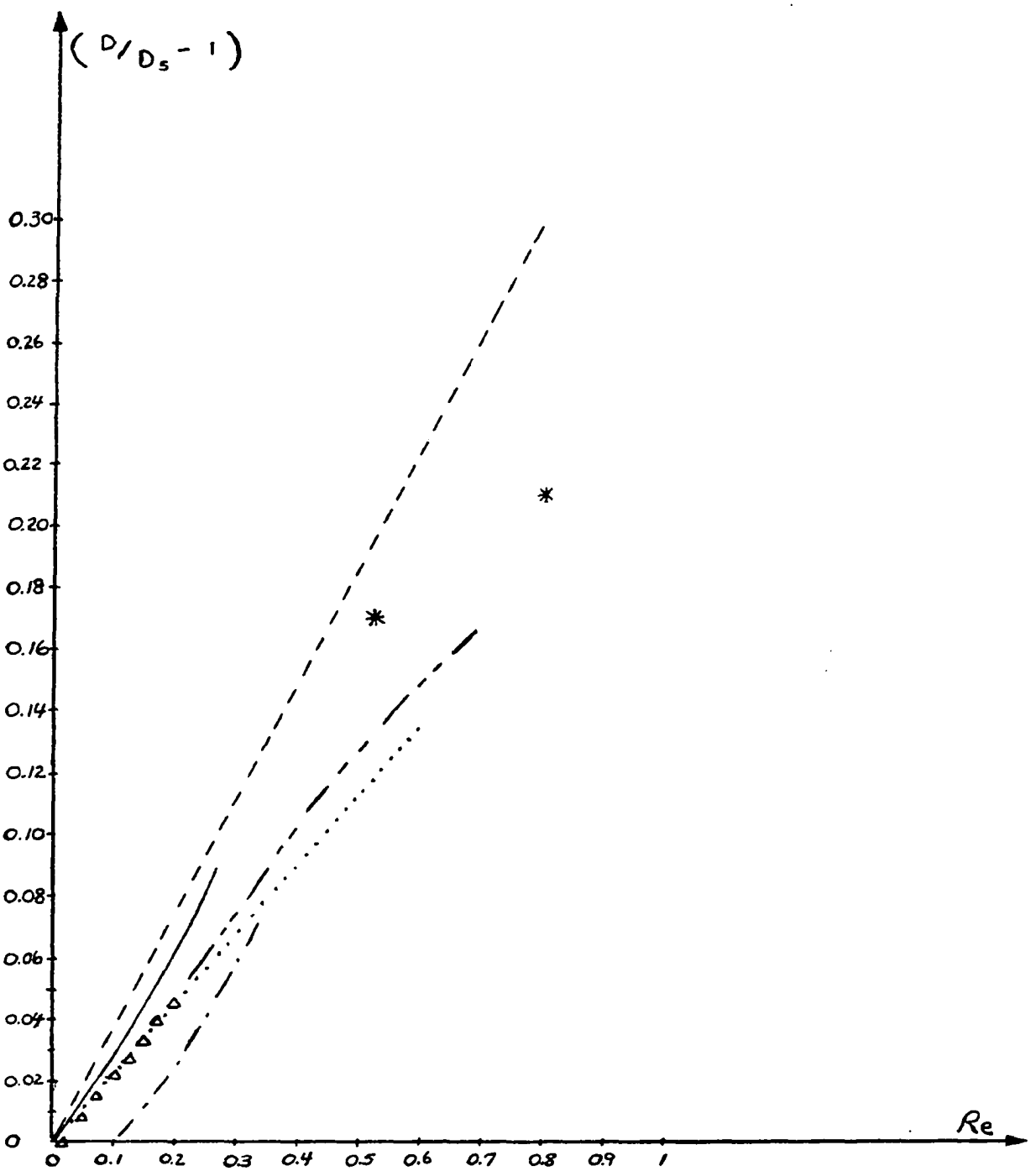


Figure 3 Variation from Stokes drag with Reynolds number.

Legend: —— Proudman-Pearson --- Oseen, * ** Maxworthy,
··· Broersma, —·— Perry, —— Castleman,
△△△ Present experimental results

CHAPTER III

EFFECT OF LINE BOUNDARIES ON SPHERE DRAG

Experimental Apparatus

The same general experimental arrangement was used for this phase of the investigation as that described in Chapter II. The only difference was the presence of line boundaries in the fluid. These boundaries were simulated by lowering monofilament nylon strings into the fluid in such a manner that they were parallel to the fall-tube axis, and at a known horizontal distance, s, from the axis.* The manner in which this distance was determined will be discussed below. The strings were heavily weighted at the lower end so that they would maintain a fixed position in the oil as the sphere passed along their length.

One of the primary purposes of this investigation was to find the correction to Stokes' law as a function of the ratio of the sphere radius to the distance of the string center from the sphere center, r/s. Thus, the diameter of the strings used was chosen to be much smaller than that of the smallest sphere used, so that any effect of their diameter could be ignored in a first order analysis. The ratio of the

---

*The axis of the fall-tube had been carefully aligned to coincide with the container axis previously.

string diameter chosen to the diameter of the smallest sphere used was $0.018/0.236 \simeq 0.076$. Also, these thin cords produced such a small change in the volume of the fluid that no essential temperature change was introduced by their presence.

In order to provide for exact string placement, and to allow the removal of the strings during a given experimental run, the following mechanism was constructed. A cylindrical aluminum shell was mounted on the ball dropping mechanism in such a way that its top was several centimeters below the large plate which held the sphere dropping disks, and its bottom was approximately 15 centimeters above the lower tip of the fall-tube. The axis of the shell was aligned to the axis of the fall-tube to within 0.001 cm. Next, twelve commercially threaded, ¼ in. diameter rods were inserted horizontally through the perifery of the shell at equally spaced intervals through the full 360° range. The axes of these rods were perpendicular to the shell surface to within 10 seconds of arc.

The holes in the shell were also threaded so that the distance from the inner tip of the rods to the fall-tube axis could be varied. Initially, it was hoped that by counting turns of the rods this distance could be fixed rather exactly for several rods simultaneously. However, the quality of the threading was such that variations in the relative rod distances as large as 0.02 cm were observed. Thus, a nut was brazed onto each rod at a position along its length such that, when this nut was flush against the outside of the shell and "locked" into place by means of a nut drawn up to the inside surface of the shell, the tip of each rod was $\sim 0.561 \pm 0.001$ cm from the fall-tube axis.

Next, several sets of twelve spacers were machined to slide on the rods between the outside of the shell and the fixed nut. Each spacer in a given set was the same length to within 0.001 cm. Thus, the distance of each rod from the central axis could be increased in fixed proportion to the other rods. Finally, each rod tip was notched in exactly the same way so that the nylon strings could slide along this tip down into the oil. The strings were run up to a pulley system over the tank, and then out through the viewing window, so that they could be raised or lowered without entering the room. Table 24 shows the actual s - distances that were achieved in this manner as determined to 0.001 cm by a measuring microscope with the strings in place.

Fall Time Determinations

Procedure

During the planning of this experiment, several methods for making the fall time determinations were considered. Ideally, the effect of the line boundaries could be found by timing two falls of the same sphere along the same path and at the same temperature, once in the presence of the line boundaries and once with no line boundaries present. Calling t_n the time for the sphere to fall with n line boundaries present, and t_0 the time with no line boundaries present, Eq. (13) gives

$$t_n/t_0 = (1 - \beta_n\, r/s), \tag{32}$$

Table 24. Horizontal Distance from Fall Line of Spheres to Line Boundaries

Rod Position	s (cm)
no spacers	0.609
no spacers*	0.638
0.5 cm spacers	1.060
1.0 cm spacers	1.561
1.5 cm spacers	2.061
2.0 cm spacers	2.561
2.5 cm spacers	3.060
3.0 cm spacers	3.561

*As mentioned in Chapter II, two fall-tubes were used. Thus, when the fall-tube of largest outside diameter was used, the "no spacer" distance was somewhat larger than indicated in the table.

provided the second order effects for the two falls are ignored. However, the experimental setup was such that, once a given sphere was dropped, the room would have to be entered and the sphere retrieved before it could be dropped again. Clearly, such a process would have destroyed the thermal equilibrium of the fluid, and, by the time this equilibrium was again reached, the temperature would quite likely be different.

Another method, involving no difficulty in experimental technique, would have been to drop a given set of spheres with the lines present on one day, and then drop the same set of spheres without the lines present on another day. According to Eq. (19), the ratio of the times found for a given sphere in this manner would be given to first order by

$$t_n^A/t_0^B = \frac{\eta^A \Delta\rho^B}{\eta^B \Delta\rho^A}\,(1 + \beta_n \cdot r/s) \ , \qquad (33)$$

where the superscripts A and B refer to the first day and the second day, respectively. However, as the error analysis in Chapter II concerning the calculation of the uncorrected viscosity clearly showed, $\Delta\rho$ and η are the least well-known quantities of all.

With the above considerations in mind, a compromise technique was devised to provide the magnitude of this effect as accurately as possible within the limitations of the experimental arrangement. For each precisely calibrated sphere, as described in Chapter II, several other spheres were chosen whose parameters closely matched those of the standard. Then, at intervals all during the course of the experiment,

certain runs were used to calibrate the fall times of these spheres relative to the standard.* Thus, calling t_s the time of fall of the standard sphere and t_m the time of fall of the mth secondary sphere, both dropped on day A, Eq. (19) shows that the ratio of these two times will be given by

$$\left(\frac{t_s}{t_m}\right)_A = \frac{r_m^2 \Delta\rho_m}{r_s^2 \Delta\rho_s} \frac{(1+\alpha Re_s)_A (1+2.1\ r_s/L)}{(1+\alpha Re_m)_A (1+2.1\ r_m/L)} \quad . \tag{34}$$

Then, once the above ratio is known, if the mth sphere is dropped on day B, and a time $(t_m)_B$ is measured, the time that the standard sphere would have taken is simply

$$(t_s)_B^{est.} = \left(\frac{t_s}{t_m}\right)_A (t_m)_B \ , \tag{35}$$

where the superscript "est." indicates that $(t_s)_B$ is not a directly measured quantity. According to Eqs. (19) and (34), Eq. (35) can be written as

$$(t_s)_B^{est} = \frac{9\,\ell\,\eta_B}{2 r_s^2 \Delta\rho_s g} \cdot \frac{(1+\alpha Re_s)_A}{(1+\alpha Re_m)_A} (1+\alpha Re_m)_B (1+2.1\ r_s/L) \ . \tag{36}$$

On the other hand, if the standard sphere had been dropped on day B, its fall time according to Eq. (19) would be

---

*The temperatures associated with these calibration runs covered the entire temperature range of the experiment (20.00 C to 23.50 C).

$$(t_s)_B = \frac{9\,\ell\,\eta_s}{2r_s^2\Delta\ell_s g}\,(1+\alpha Re_s)_B(1+2.1\,r_s/L)\ .$$

Thus, the ratio of the estimated time of fall of the standard to the rate at which it would have fallen on day B is given by

$$\left(\frac{t_s^{est}}{t_s}\right)_B = \frac{1+\alpha(Re_s)_A}{1+\alpha(Re_m)_A}\cdot\frac{1+\alpha(Re_m)_B}{1+\alpha(Re_s)_B}\ . \qquad (37)$$

By expanding Eq. (37) to first order in Re, and replacing each Re value by the basic parameters, it follows that, for any day B,

$$\frac{t_s^{est}}{t_s} \simeq 1 + \alpha\ell\left[\left(\frac{\rho_A}{t_{s,A}\eta_A} - \frac{\rho_B}{t_{s,B}\eta_B}\right)r_s - \left(\frac{\rho_A}{t_{m,A}\eta_A} - \frac{\rho_B}{t_{m,B}\eta_B}\right)r_m\right]\ . \qquad (38)$$

The sphere having the largest fall times and the lowest Re values is 1/8 PP. When the parameters associated with this sphere and the fluid, over one-half the temperature range of the experiment, are inserted into Eq. (38), it is found that $(t_s)^{est} = t_s(1 \pm 5 \times 10^{-6})$. Thus, using the typical t_s(1/8 PP) value of 400 sec, it should be possible to determine t_s(1/8 PP) in this manner to within 0.002 sec. A similar estimate of $\sim$0.002 sec is also found for all the other spheres. Since these differences are much smaller than the accuracy of $\pm$0.05 sec with which the times were measured, the procedure was justified.

While the actual timing error for a single measurement of the ratio t_s^{est}/t_s is $0.01/t_s$, the results of from 7 to 9 calibration runs for each secondary sphere gave a mean value of this ratio whose standard deviation of the mean was of the order of the error for a single time measurement, namely 0.05 sec. In fact, these results were so good that a number of $(t_s)^{est}$ times were used in the analysis discussed in Chapter I. In all cases the $(t_s)^{est}$ values used there were found to lie on the curve, within the allowed experimental error, formed by the t_s values.

Technique

In order to achieve the spirit of the ideal procedure leading to Eq. (32), the following experimental technique was used. In setting up a given run, the first six slots of the twelve-slot disk on the ball-drop mechanism were used to hold a certain variety of sphere types, e.g. 1/8 PP_l, 3/32 N_s, 3/16 PP_s, 1/4 PP_l, 5/32 N_l, and 3/16 N_s. Then the second six slots were used to hold an identical variety of sphere types, e.g. 1/8 PP_s, 3/32 N_l, 3/16 PP_l, 1/4 PP_s, 5/32 N_s and 3/16 N_l.

After loading the ball-drop mechanism, the string configuration to be used in the next run was set up and lowered into place in the tank. Then the container room was locked up and allowed at least twelve hours to reach thermal equilibrium. As soon thereafter as a constant temperature was found to exist in the room, the run was begun.

In this way the first six spheres were timed, with appropriate time intervals between each fall as discussed in Chapter II, in the vicinity of a particular string configuration. At this point the strings were slowly raised up out of the oil, using the pulley mechanism discussed earlier, until the weights on their ends were entirely out of the oil, and the tank thermometer was lowered into position in the oil. Since convective currents were set up by raising the strings out of the fluid, a time interval of approximately thirty minutes was allowed to pass with the tank thermometer still in place. Then, if the tank thermometer showed the same temperature as the recorded value when the run was initiated, it was very slowly pulled up, and another time interval of 10 to 15 minutes was allowed to elapse before the next sphere was dropped. Thus, the remaining spheres were timed with no line boundaries present at a temperature essentially identical to that during the fall of the first six spheres.* Finally, at the end of the run, the tank thermometer was again lowered into place and its temperature observed. Only one run out of more than forty had to be thrown out due to a noticeable temperature difference before and after the run.

---

*For the initial run, the first six spheres were allowed to fall in the absence of one string, which was then lowered into the tank during the run. However, this procedure gave rise to tiny air bubbles along the string which took several hours to rise to the surface. Also, by lowering the strings into the oil before a run was begun, their placement could be checked and any necessary corrections made.

Tables 25, 26, 27, 28 and 29 show the t_s and t_s^{est} values determined in this manner. When more than one string is present in the fluid, they were all placed at the same distance, s, from the fall axis, as indicated by the r/s values given in these tables. The β_n values that appear have been calculated from Eq. (32) as a first order estimate. Finally, for later reference, the associated value Re_0 for each fall without the boundaries present has been included in the tables.

Table 30 lists the mean value of each β_n, and the standard deviation from each mean.

Table 25. One String Runs

T(°C)	t_1(sec)	t_0(sec)	t_1/t_0	r/s	β_1	Re_0
			1/8 PP Sphere			
20.50	435.84	416.24	1.047	0.26	0.179	0.006
23.65	330.65	316.45	1.044	0.25	0.178	0.010
23.00	344.60	335.54	1.027	0.15	0.178	0.009
			3/32 N Sphere			
22.40	69.17	66.85	1.034	0.19	0.178	0.032
23.65	62.54	60.54	1.033	0.18	0.178	0.039
23.00	65.02	63.76	1.019	0.11	0.178	0.035
			3/16 PP Sphere			
20.70	216.58	203.20	1.065	0.37	0.178	0.018
19.50	239.65	224.90	1.065	0.37	0.177	0.016
23.65	168.82	158.50	1.065	0.37	0.176	0.029
23.00	172.56	166.09	1.038	0.22	0.174	0.027
			1/4 PP Sphere			
19.50	138.53	127.60	1.085	0.49	0.173	0.036
20.70	123.30	113.45	1.086	0.49	0.175	0.045
23.65	94.92	87.50	1.084	0.49	0.171	0.073
23.00	97.59	92.77	1.051	0.29	0.174	0.065

Table 25 (Cont'd.)

1/8 N Sphere

23.65	36.51	34.91	1.045	0.24	0.186	0.089
23.00	37.41	36.48	1.025	0.14	0.172	0.081

5/32 N Sphere

23.65	23.49	22.42	1.047	0.30	0.154	0.168

Table 26. Two String Runs

T(°C)	t_2(sec)	t_0(sec)	t_2/t_0	r/s	β_2	Re_0
			1/8 PP Sphere			
21.40	416.33	385.85	1.078	0.25	0.314	0.007
22.30	384.40	356.12	1.079	0.25	0.316	0.008
23.45	336.97	321.57	1.047	0.15	0.317	0.009
23.55	330.07	319.53	1.032	0.10	0.320	0.009
			3/32 N Sphere			
21.20	77.30	73.00	1.058	0.18	0.318	0.027
22.30	72.29	67.34	1.073	0.18	0.397	0.031
23.45	63.75	61.64	1.034	0.11	0.308	0.037
23.55	62.42	61.06	1.022	0.07	0.293	0.038
			3/16 PP Sphere			
21.05	220.31	197.44	1.115	0.37	0.313	0.019
21.40	212.85	190.93	1.114	0.37	0.310	0.021
23.45	171.69	160.43	1.070	0.22	0.314	0.028
23.55	166.55	159.09	1.046	0.15	0.310	0.029
			1/4 PP Sphere			
21.05	126.64	110.06	1.150	0.49	0.304	0.047
21.40	122.79	106.70	1.150	0.49	0.304	0.050

Table 26 (Cont'd.)

22.22	114.45	99.41	1.151	0.49	0.305	0.057
23.45	97.29	89.13	1.091	0.29	0.307	0.070
23.55	93.64	88.20	1.061	0.20	0.305	0.071
			1/8 N Sphere			
22.30	41.29	38.34	1.076	0.24	0.312	0.075
23.45	37.85	36.10	1.048	0.14	0.327	0.088
23.55	36.21	35.17	1.029	0.10	0.292	0.089
			5/32 N Sphere			
22.20	27.46	25.18	1.090	0.30	0.293	0.139
			3/16 N Sphere			
22.20	20.10	18.20	1.104	0.37	0.282	0.232
23.55	17.34	16.59	1.043	0.15	0.287	0.274

Table 27. Four String Runs

T(°C)	t_4(sec)	t_0(sec)	t_4/t_0	r/s	β_4	Re_0
			1/8 PP Sphere			
22.70	391.15	344.02	1.137	0.25	0.545	0.008
21.80	423.72	372.64	1.137	0.25	0.546	0.007
21.83	406.08	374.84	1.083	0.15	0.551	0.007
21.00	422.87	400.09	1.056	0.10	0.552	0.006
21.55	396.12	379.70	1.043	0.07	0.554	0.007
20.52	430.76	416.16	1.035	0.06	0.556	0.006
20.10	442.03	431.29	1.024	0.04	0.553	0.006
			3/32 N Sphere			
21.80	76.91	69.78	1.102	0.18	0.552	0.029
21.50	78.54	71.28	1.101	0.18	0.550	0.028
21.83	73.78	69.58	1.060	0.11	0.543	0.029
21.00	77.00	73.88	1.042	0.07	0.555	0.026
20.10	80.21	78.75	1.018	0.03	0.561	0.023
			3/16 PP Sphere			
22.70	204.30	170.71	1.196	0.37	0.531	0.025
21.60	223.72	187.56	1.192	0.37	0.521	0.021
21.50	226.50	189.38	1.196	0.37	0.529	0.021
21.83	206.45	184.00	1.220	0.22	0.547	0.022

Table 27 (Cont'd.)

21.00	214.57	198.04	1.083	0.15	0.552	0.019
21.55	200.60	188.67	1.063	0.11	0.549	0.021
20.60	215.63	205.24	1.050	0.09	0.550	0.018
20.52	216.83	206.32	1.050	0.09	0.553	0.018
20.10	222.25	214.32	1.037	0.06	0.560	0.017
			1/4 PP Sphere			
22.70	119.39	95.38	1.251	0.49	0.508	0.071
21.80	128.44	102.63	1.251	0.49	0.508	0.054
21.50	132.39	105.80	1.251	0.49	0.507	0.051
21.83	119.10	102.88	1.157	0.29	0.529	0.054
21.00	122.57	110.61	1.108	0.20	0.535	0.047
21.55	114.21	105.40	1.083	0.15	0.546	0.051
20.10	124.63	118.88	1.048	0.08	0.543	0.041

Table 28. Six String Runs

T(°C)	t_6(sec)	t_0(sec)	t_6/t_0	r/s	β_6	Re_0
			1/8 PP Sphere			
20.62	457.47	412.23	1.109	0.15	0.726	0.006
			3/32 N Sphere			
20.62	82.05	75.90	1.081	0.11	0.730	0.024
			3/16 PP Sphere			
20.62	237.67	205.10	1.158	0.22	0.712	0.018
			1/4 PP Sphere			
20.62	138.14	114.49	1.206	0.29	0.693	0.044

Table 29. Twelve String Runs

T(°C)	t_{12}(sec)	t_0(sec)	t_{12}/t_0	r/s	β_{12}	Re_0
			1/8 PP Sphere			
21.25	456.48	390.52	1.168	0.15	1 118	0.006
20.57	451.00	414.06	1.089	0.07	1.143	0.006
19.85	480.14	440.81	1.089	0.07	1.143	0.005
20.80	430.50	406.23	1.059	0.05	1.148	0.006
20.00	460.77	434.79	1.059	0.05	1.149	0.005
			3/32 N Sphere			
21.25	81.72	72.60	1.125	0.11	1.131	0.027
22.25	73.44	67.57	1.086	0.07	1.143	0.031
21.50	75.93	71.28	1.065	0.05	1.144	0.028
20.57	81.21	76.23	1.065	0.05	1.146	0.024
19.85	85.66	80.41	1.065	0.05	1.145	0.022
20.80	77.74	74.40	1.044	0.03	1.151	0.022
			3/16 PP Sphere			
21.25	240.19	193.59	1.240	0.22	1.079	0.020
22.30	207.10	177.22	1.168	0.15	1.116	0.024
21.50	214.01	189.38	1.130	0.11	1.130	0.021
20.57	232.63	205.85	1.130	0.11	1.131	0.018

Table 29 (Cont.d)

19.85	247.37	218.90	1.130	0.11	1.131	0.016
20.80	219.46	201.72	1.087	0.07	1.142	0.019
20.00	235.06	216.07	1.087	0.07	1.141	0.016
			1/4 PP Sphere			
21.25	140.86	108.03	1.303	0.29	1.019	0.048
20.40	141.62	116.21	1.218	0.20	1.082	0.043
22.25	120.59	99.00	1.218	0.20	1.079	0.057
21.50	123.69	105.80	1.169	0.15	1.105	0.051
20.57	134.20	114.77	1.169	0.15	1.106	0.044
19.85	142.06	121.48	1.169	0.15	1.107	0.039
20.80	125.47	112.44	1.115	0.10	1.125	0.045
20.00	133.96	120.04	1.115	0.10	1.125	0.040

Table 30. Best β_n Values from First Order Calculation

String Number (n)	$\bar{\beta}_n$	$\sigma(\beta_n)$
1	0.176	0.003
2	0.311	0.009
4	0.543	0.006
6	0.716	0.017
12	1.123	0.012

Variation of Sphere Drag with Number of Lines

The most obvious effect shown by Table 30 is the increase in $\bar{\beta}_n$ as the number of lines surrounding the sphere's fall line was increased. Figure 4 gives a graphic display of this increase. Certainly, the qualitative features of the resultant curve are not unexpected.

A single line gives rise to a definite interaction of the fluid with the sphere which results in an increase in the drag force exerted by the fluid on the sphere. With two lines on opposite sides of the sphere, each at a distance large compared to the sphere radius, their combined effect might well be independent to first order. This supposition is apparently not verified within the error limits shown in Table 30; although the interaction is seen to be small.

As more lines are added, the interaction between the lines should become more and more apparent, which is evidently verified by the 4, 6 and 12 line cases. The tapering off of the curve in Fig. 4 is definitely to be expected, since $\bar{\beta}_n$ should approach Faxén's value of 2.1 as $n \to \infty$. Perhaps the only surprising result in this figure is that the increased drag on the sphere is over half the expected Faxén value when n is just twelve.

Since no known theoretical treatment of this effect exists in the literature, its quantitative aspects are deferred to the final section of this paper, where the theoretical consequences of line boundaries are considered in general.

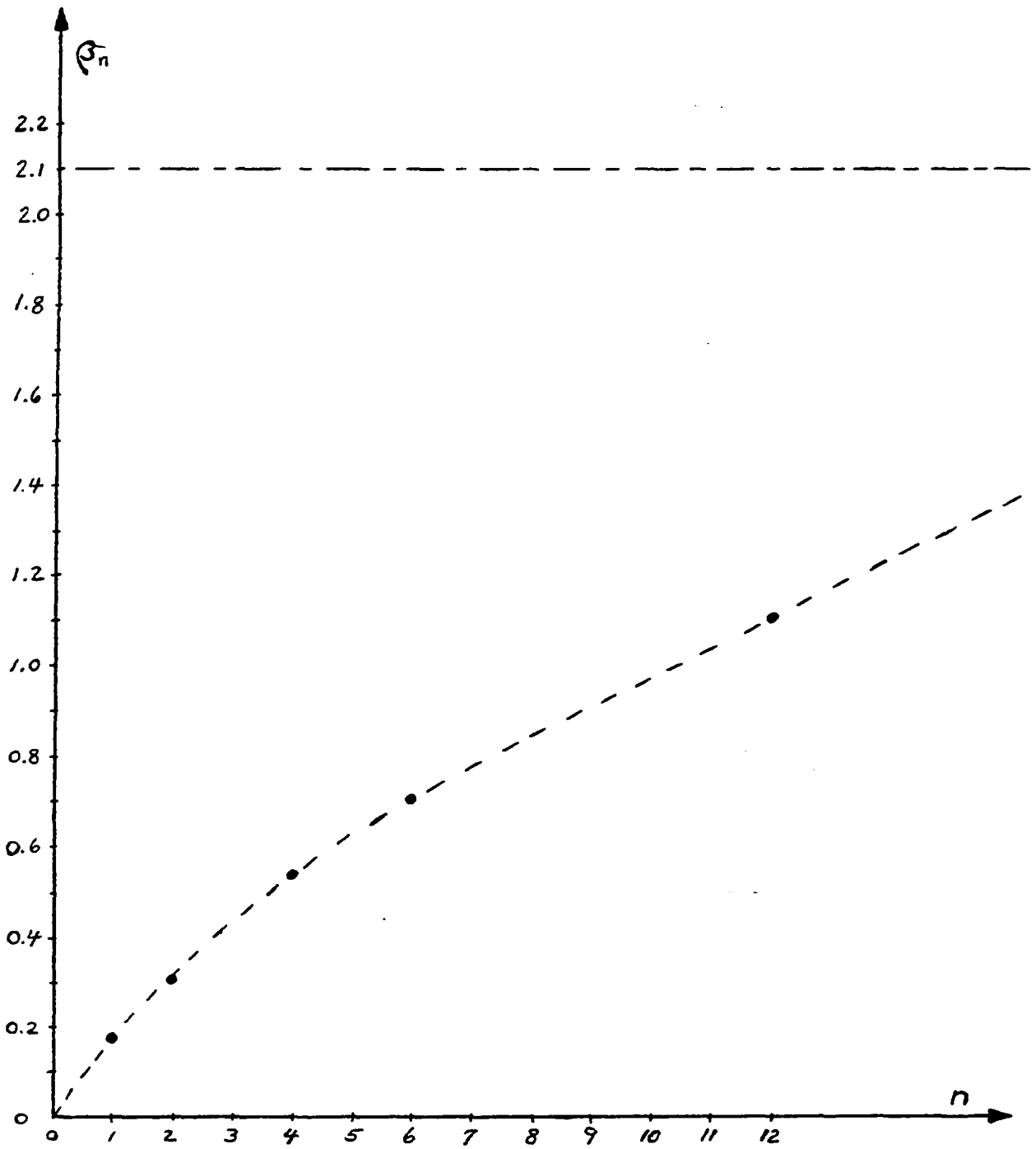


Figure 4. Variation in Sphere drag with String number.

Legend: ... experimental points, --- projected change in β_n with string number, ——— line giving the value of β_n that should be approached as $n \to \infty$.

Theoretical Analysis

Impossibility of Exact Boundary Match Between a Sphere and a Line

The most straight forward approach to the problem of predicting the increased drag on a sphere due to some particular configuration of line boundaries would be to solve the Stokes' equations given by (5a,b) for the velocity field, and then match the arbitrary constants in the solution to both the sphere and the line boundaries subject to the condition that the field remain finite at infinity. Clearly, the usual axisymmetric solution used for finding the drag force on a sphere in an unbounded medium will not be general enough in this case, due to the asymmetry introduced by certain line configurations.

The solution to Stokes' equations is given in general terms by Lamb.[31] Using his results, the velocity field can be put in the form

$$v_r = \sum_{n,m}(-1)^n \left\{B_{nm}(-n-1)\left(\frac{a}{r}\right)^{n+2} + C_{nm}\frac{n(n+1)}{2n(2n-1)}\left(\frac{a}{r}\right)^n\right\}\cos m\phi\, P_n^m, \tag{40a}$$

$$v_\theta = \sum_{n,m}(-1)^n \left\{B_{nm}\left(\frac{a}{r}\right)^{n+2}P^m_{n,\theta} + D_{nm}\left(\frac{a}{r}\right)^{n+1}\frac{P_n^m}{\sin\theta} + C_{nm}\frac{2-n}{2n(2n-1)}\left(\frac{a}{r}\right)^n P^m_{n,\theta}\right\}\cos m\phi, \tag{40b}$$

$$v_\phi = \sum_{n,m}(-1)^n \left\{B_{nm}(-m)\left(\frac{a}{r}\right)^{n+2}\frac{P_n^m}{\sin\theta} + D_{nm}\left(\frac{a}{r}\right)^{n+1}P^m_{n,\theta} + C_{nm}\frac{-m(2-n)}{2n(2n-1)}\frac{P_n^m}{\sin\theta}\right\}\sin m\phi, \tag{40c}$$

where $P_n^m \equiv P_n^m(\cos\theta)$ is the usual Legendre polynomial, $P_{n,\theta}^m \equiv dP_n^m/d\theta$ and B_{nm}, C_{nm}, D_{nm} are arbitrary constants to be determined by the boundary conditions. In the double summations, n = 0, 1, 2, ... so that the condition of a finite field at infinity is guaranteed, while m = 0, 1, 2, ..., n - 1. For the case of one vertical line at horizontal distance s from the sphere center, the appropriate boundary conditions are

$$\vec{v} = U\,\hat{k} \text{ at } r = a, \tag{41a}$$

$$\vec{v} = 0 \text{ at } \rho = 0 \text{ and } r\sin\theta = s\ . \tag{41b}$$

The boundary condition given by Eq. (41a) is easily fit to the field as expressed in spherical coordinates in Eqs. (40a,b,c). The second boundary condition, however, is incompatible with these equations. The velocity field can be transformed to cylindrical coordinates by means of a very laborous technique outlined in Happel and Brenner.[32] However, the resultant match to the line boundary would not be compatible with that on the sphere.

The general perturbation technique known as the "method of reflections" could perhaps be used to obtain a first order approximation to this problem; however, there is no guarantee that this method would work since the line boundary is not closed.[33] There still remain several "trick" techniques that might provide a crude estimate of the effect of line boundaries. One of these techniques is discussed in the following sections.

Method of Images

The method of images in fluid mechanics follows from a reciprocal theorem to the Stokes' equations. This theorem was the work of Lorentz, and can be stated in the following manner.[34] Let (v_j, Π_{ij}) and (v'_j, Π'_{ij}) be the velocity and stress fields corresponding to any two motions of the same fluid which conform to the Stokes' Eqs. (5a,b). Then

$$\int_S dS_i \Pi_{ij} v_j = \int_S dS_i \Pi'_{ij} v'_j \tag{42}$$

where S is a closed surface bounding any fluid volume V; S may consist of a number of distinct surfaces separated from each other.

Based on the above theorem, for any solution $(\vec{v}, P)$ of the Stokes' equations, a new solution is given by

$$\vec{v}' = -\vec{v} + 2u\hat{i} - 2|x|\nabla u + \frac{x^2}{\eta}\nabla p \ , \tag{43}$$

$$p' = p + 2\, x\, \nabla_x\, p - 4\eta \nabla_x\, u \ , \tag{44}$$

where $\vec{v} = (u, v, w)$. A proof of the above relations is given in Appendix A.

The primary usefulness of these new solutions arises from the fact that at $x = 0$

$$v' = v, \qquad u' = -u, \qquad w' = -w \ , \tag{45}$$

so that they represent a mirror image solution of the original solution (v, p) relative to the plane x = 0. Lorentz used this fact to find the first order drag correction both to a sphere moving toward an infinite plane and to a sphere moving parallel to an infinite plane, with the results of the former calculation being quoted in Eq. (11).

The calculation for a sphere moving parallel to an infinite plane is of definite interest here, since it will be possible to make a crude comparison between a plane and a line. Hence, an outline of this calculation will now be given. Consider a sphere of radius a moving along the z axis with velocity U, whose midpoint is located at (-s, 0, 0). The Stokes' field due to the motion of this sphere for a point force in an unbounded medium is given by[35]

$$u = -\frac{3}{4} Ua \frac{z(x+s)}{r^3} , \tag{46a}$$

$$v = -\frac{3}{4} Ua \frac{zy}{r^3} , \tag{46b}$$

$$w = -\frac{3}{4} Ua \left(\frac{1}{r} + \frac{z^2}{r^3}\right) , \tag{46c}$$

where $r^2 = (|x|+s)^2 + y^2 + z^2$. By adding this solution to its mirror image solution, one should have the appropriate field for a sphere moving parallel to an infinite plane in the region x<0. The x-component of the reflected field is found from Eqs. (43) and (46a,c) to be

$$w' = \frac{3}{4} Ua\left(\frac{1}{r} + \frac{z^2}{r^3}\right) - 2|x|\left[-\frac{3}{4} Ua(|x|+s)\left(\frac{1}{r^3} - \frac{3z^2}{r^5}\right)\right] +$$

$$+ \frac{x^2}{\eta}\left[-\frac{3}{2}\eta aU\left(\frac{1}{r^3} - \frac{3z^3}{r^5}\right)\right] . \qquad (47)$$

Evaluating this velocity component at $x = -s \Longrightarrow r = 2s$, $y = z = 0$ gives

$$w' = Ua/s(3/8 + 3/8 - 3/16) = U(9/16 \cdot a/s) .$$

Hence the z-component of the sphere's velocity relative to the fluid is $(1 + 9/16 \cdot a/s)U$ giving a total drag on the sphere of

$$D_p = 6\pi\eta aU(1 + 9/16 \cdot a/s) . \qquad (48)$$

Relation Between Plane and Line

In order to obtain an estimate of the drag force on a sphere due to its motion parallel to a rigid line boundary, it should be possible to consider the line as being made up of infinitesimal point forces. The magnitude of these point forces should be such that, if they are summed over an entire plane, the resultant effect is the same as that given by Eq. (48).

The effect of each infinitesimal point force can be represented by the proportionality[36]

$$dF_z \propto \frac{d^nA/s^n}{(\ell/s)^2}\,[(U\cos\theta)\cos\theta]\ , \tag{49}$$

where ℓ is the distance from the point to the sphere, and n represents the dimensionality of the total surface with area element d^nA under consideration, i.e., n = 3 for a sphere, n = 2 for a plane, n = 1 for a line. The factor U cosθ arises when the component of the velocity of the sphere is taken perpendicular to the line joining the sphere center to the point force, and the factor cosθ arises when the z-component of the resultant force is formed. When Eq. (49) is evaluated for a plane, the result is $\pi^2/2$; whereas, the result for a line is $\pi/2$.

Thus, the additional drag on a sphere moving parallel to a line can be estimated by

$$1/\pi \cdot 9/16 \cdot a/s \cong 0.179 \cdot a/s. \tag{50}$$

Conclusion

The theoretical analysis given above, though admittedly crude, should provide a first order comparison with the experimental results. This expectation is borne out for one string since the coefficient of a/s given by Eq. (50) is only 1.7 per cent higher than the experimental result for $\bar{\beta}_1$ as given in Table 30.

For two strings, it was noted in the discussion of Table 30 that the effect of two strings was not quite twice that of a single string. The case of a sphere moving between parallel planes has been treated by Faxen with the result to first order being given by[37]

$$D_2 = 6\pi\eta\, aU(1 + 1.004 \cdot a/s) \quad . \qquad (51)$$

When the coefficient of the a/s term given above is again divided by π, the result is 0.320 as compared to 0.311 found from experiment. The difference between these two values is only 5 per cent, which is good agreement for a first order approximation. It should be remembered that the experimental values as calculated in Table 30 do ignore the higher order effects that were necessarily present in the actual sphere fall. Unfortunately, the accuracy in timing the spheres was not great enough to justify a higher order analysis. However, it would be expected that the experimental values for the β_n would be slightly higher since the series in a/s usually alternates in sign.[40] The situation is complicated, however, by the fact that, to the second order in a/s (if the second order occurs at all), the first order effects of the string size, the outer boundary and fluid inertia must be considered.

For the larger string numbers, the comparison between planes and lines would probably not be quite as close to that found above, unless some account could be taken of the difference in the interactions between the planes as compared to those between the lines. However,

such a comparison is not possible at this time since results for higher numbers of planes are not available in the literature.

In conclusion, the effect of increased sphere drag as measured earlier appears to be quite close to the predictions that follow from the Stokes' equations.

Appendix A

It is to be proved here that given a field $(\vec{v},p)$ satisfying the Stokes' equations

$$\eta\nabla^2\vec{v} = \nabla p, \qquad \nabla\cdot\vec{v} = 0 ,$$

the field given by

$$\vec{v}' = \vec{v} + 2u\hat{i} - 2x\nabla u + \frac{x^2}{\eta}\nabla p ,$$

$$p' = p + 2x\nabla_x p - 4\eta\nabla_x u ,$$

is also a solution to Stokes' equations.

Using the fact that

$$\nabla^2\vec{v} = \nabla_\Lambda\nabla_\Lambda\vec{v}$$

for $\nabla\cdot\vec{v} = 0$, it is a simple matter to show that

$$\eta\nabla^2\vec{v} = \eta\nabla_\Lambda\nabla_\Lambda\vec{v} - 2\eta\nabla\nabla_x u + 4\eta\nabla^2 u\hat{i} - 2\eta\,\nabla_x\nabla u - 2(\nabla^2 p)x\hat{i} + 2\nabla p -$$

$$- 2\nabla_x p\hat{i} + 2x\nabla_x\nabla p .$$

On the other hand,

$$\nabla p' = \nabla p + 2\hat{i}\nabla_x p + 2x\nabla\nabla_x p - 4\eta\nabla\nabla_x u .$$

Since $\nabla^2 p = 0$, $\eta\nabla^2\vec{v} = \nabla p$ and $\eta\nabla^2 u = \nabla_x p$, it is easily seen that

$$\eta\nabla^2\vec{v}' = \nabla p' .$$

These same facts can be used to easily varify the relation

$$\nabla\vec{v}' = 0 .$$

Appendix B

Simultaneous Translation and Rotation of Bodies at Low Reynold's Numbers

History of the Problem

The so-called lift forces, associated with a body undergoing both translational and rotational motion through a material medium, have been a scientific curiosity since the time of Sir Isaac Newton, if not longer.[39] Newton mentioned having observed the effect in the game of tennis, and gave his explanation as follows: "... for its parts on that side where the motions conspire must press and beat the contiguous air more violently than on the other; and there excite a reluctancy and reaction of the air proportionably greater ... ." He then proceeded to make an analogy between this effect and his corpuscular theory of light, thinking perhaps that some of the bending of the paths of these corpuscles in a prism might be accounted for in this manner; however, he gave no quantitative treatment of the problem.

No further discussion of this problem appears in the literature until after the middle of the nineteenth century. At approximately that time a cannon maker named Robbins performed some qualitative experiments by bending the muzzel of his cannons and observing the resultant motions of the cannon balls, which, he claimed, tend to move in a direction opposite to the bend in the muzzle.[40] The first person to claim the equivalence between the motion of a simultaneously rotating and translating body in a fluid to that of a

rotating body placed in a steady stream of fluid was Euler.[41] His argument was "... if the ball has a progressive motion we may ... consider it at rest, and the air flowing against it with the velocity of the ball's motion; for the force with which the particles of air act on the body will be the same in both cases." On the basis of his investigations, Euler came to the conclusion that Robin's work had been faulty and that "if, therefore, such a ball should receive two such motions in the cannon, yet its progressive motion in the air will be the same as if it has no rotation." Poisson later came to the erroneous conclusion that, "since friction is greater where the density of air is greater, the front of the ball suffers greater friction than the back; thus, there is a lateral force, which shows to be very small, tending to deflect the ball as if it were rolling upon the air in front of it."[42]

In 1890, P. G. Tait carried out an analysis of this problem based on the assumption that the fluid medium would exert a resistance on the ball proportional to the square of the linear velocity plus some small portion of the angular velocity.[43] It would then follow that the deflecting force would vary as the product of the linear and angular velocities. He received confirmation of his reasoning from Sir G. G. Stokes. He also performed numerous experiments with golf balls and found fair agreement with his theoretical calculations.

The first treatment of this problem from the standpoint of pure hydrodynamics was due to Proudman in 1916 and Taylor in 1917.[44,45] However, their analyses were based on the assumption of a perfect fluid and could only be expected to apply to large Reynold's number motions. Therefore, though such motions have been given a good deal more mathematical and experimental consideration than low Reynold's number motions, their results will not be discussed here. The remainder of this section will deal with only those analyses of low Reynold's number motions.

The first analysis of the lift forces involved in low Re number motion was due to Garstang in 1933.[46] Realizing that lift forces based on the interaction of two modes of body motion could not possibly be associated with the Stokes' equations due to their linearity, he chose to work with the Oseen equations. These equations were solved for both spheres and cylinders, and he found that neither the torque nor the drag on these bodies would differ from that found when they possessed either translational or rotational motion separately. In the case of the sphere, he immediately ruled out a lift force associated with "side spin", i.e., the spin axis in the direction of the translation, on the basis of symmetry. His results for a sphere having "top spin", i.e., its spin axis perpendicular to the translational motion, were rather confusing. The evaluation of the associated lift force by means of integrals at infinity gave zero lift, while integrals over the body surface gave a force in the opposite direction to that predicted earlier for ideal fluids. A similar state

of confusion resulted from the cylinder calculations. Evaluation of the associated lift forces by means of integrals at infinity gave a result in accordance with ideal fluid theory; whereas, integrals over the body surface gave only one half that value. In his concluding remarks he stated that "the discrepancy and disagreement of the results with observation show that if Oseen's equations are used to determine coefficients from boundary conditions, we cannot rely upon obtaining a good approximation of the motion either near the solid or at infinity." He also noted the fact that there was no way to make direct comparisons between his results and experiment since no motions of this type in the low Reynold's number range had ever been measured.

In 1961, the Kaplan technique, as explained in the Introduction, was applied by Rubinow and Keller to obtain the lift on a sphere.[47] By taking the spin axis to have an arbitrary, but fixed, orientation throughout the calculation, they were able to give their result in vector form according to the relation

$$\vec{F}_L = \pi \rho a^3 \vec{U} \times \vec{\Omega}, \tag{52}$$

where $\vec{U}$ is the stream velocity and $\vec{\Omega}$ is the angular velocity of the sphere. This result is one fourth as large as the result predicted by ideal fluid theory for large Re.

It is of interest to note that as of the beginning of 1969, eight years later, no experimental investigation of the above effect has yet appeared in the literature. Also, no one has yet published an expression for the low Reynold's number lift on a cylinder, and no experimental work of this nature has been published.

Preliminary Experimental Work

The fluid medium used in almost all of the investigation was Whiterex - 344, whose properties were described in Chapter II. Several runs were also made with castor oil. The body symmetries used were both cylindrical and spherical. The cylindrical bodies were those used by Dodson in his work; whereas, the spherical bodies were obtained in department stores and were quite crude.[48]

The original apparatus constructed for these experiments was designed to give simultaneous readouts of the torque, drag, and lift on the body. It also allowed the rigid body to move with three translational degrees of freedom and one rotational degree of freedom. Two of the translational degrees of freedom and the rotational degree of freedom were driven externally in a fashion that was to still allow individual changes in these motions, due to the interaction of the body with the fluid medium, to be measured. In this way it would have been possible to simulate something as complicated as Brownian motion.

Unfortunately, the mechanical constraints necessary to create the driving motions never could be made to operate without causing interactions with the body motion that in some cases were larger than the fluid interaction that was to be measured. In addition, the method of taking measurements with this device did not work out quite as well as expected. This method involved the creation of a permanent record by means of an electrical spark between a sharp point and a plane. There was always the problem of linearity between the spark and the line of the sharp point, especially after the device had been

sparked several times and had pitted the surface of the plane. I still believe this recording device could have been made to work; however, the mechanical difficulties were never resolved before it was concluded that another approach might give some of the desired results in a more realistic length of time.

At this point it was evident that external mechanical interactions would have to be minimized as much as possible. Certainly, the timing of bodies undergoing free-fall in a fluid medium meets the above criterion, and, as such, constitutes the most frequently used technique of obtaining precise results in the field of low Reynold's number hydrodynamics. However, the problem still remained of creating a simultaneous rotational motion of the body, with the axis of rotation perpendicular to the line of the translational motion caused by the constant gravitational field. Two such ways were eventually used, each having its own advantages and disadvantages.

The first technique devised to create simultaneous rotation and translation involved the use of the common yo-yo configuration. It is an established fact that trying to drag a string, connected to the body, through the medium causes more problems than it solves. However, in the yo-yo the string, attached to a fixed upper support, simply unwinds from the spindle so that very little motion of the string should take place. Thus, the deviation of the line of motion of the yo-yo from the line connecting the center of mass of the ball to the point of the fixed support (which would define the vertical

along which the yo-yo would fall in a vacuum) should give a measure of the lifting force associated with the motion of the yo-yo.

However, experimentation with this device soon showed that the situation was more complicated than had at first been thought. This complication arises from the fact that the rotational motion of the medium in the vicinity of the yo-yo's surface causes a deviation from the straight line in string coming up from the yo-yo to the fixed support, which was not accounted for in the paragraph above. This deviation varied with the magnitude of the rotational motion of the yo-yo; but, in most cases it appeared that the string did not lose contact with the yo-yo spindle at that point where a straight line from the fixed support just lines up with the tangent line of the spindle (as it should do when the yo-yo falls in a vacuum). Rather, the string continued to cling to the yo-yo for a short arc length above this tangent point. Then, starting from that point at which the string left the yo-yo spindle, it rather quickly curved up toward the point of support. The overall effect of this string bend was to create a tangent line running from the fixed support down to the yo-yo that more nearly intersected the center of mass of the yo-yo than the outer tangent of the spindle. Calling the angle of the string's deviation from the vertical ε, it is a simple matter to show that, for $\alpha \ll 1$, its theoretical value should be given by

$$\varepsilon_{th} \simeq F_L/(mg-D). \quad (53)$$

*There was one other complication here. As the string of finite radius was wound around the yo-yo spindle, it was necessary to try to alternate the turns on either side of the geometric center, since otherwise the yo-yo would rotate about a vertical axis as it fell.

The alternate technique used to create simultaneous translation and rotation of the body was achieved in the free-fall of a body whose center of mass did not coincide with its geometric center. If the center of mass of the body is almost vertically above its geometric center when the body is dropped, it is possible to have the body rotate through almost 180° as it falls. This implied a slow rate of rotation over a decent fall length which proved to be a detriment to the experimental runs utilizing this effect. A complete analysis of the time dependent motion of such bodies was not found necessary, since, to a very good approximation, the horizontal motion of the bodies used very rapidly reached a steady state condition. This state of motion implies that the horizontal component of the lifting force was just balanced by the horizontal component of the dragging force. Thus, the angle of deviation should have the value

$$\varepsilon_{th} \simeq F_L/F_D, \qquad \varepsilon<<1 \ . \tag{54}$$

The technique used to determine the angle of deviation of the bodies' motion from the vertical consisted of photographing the motion through a light chopper rotating at a known rate. Two exposures of each plate were made, with the second exposure defining the vertical. The developed plates were then analyzed by means of a measuring microscope. In all cases the bodies fell in rather small fishtanks whose seams had been coated with epoxy to keep the oil from seeping out. However, it was not possible to isolate the tank thermally. This

fact, coupled with the difficulty of determining the cylinder drag and the lack of sphericity of the spheres, precluded the attainment of high precision in the measurements. Sample results for the spheres and cylinders are summarized and discussed separately.

Table 31 shows fair agreement with the relation given by Rubinow and Keller. Even though the experimental accuracy leaves much to be desired, it definitely appears that the Rubinow and Keller relation is to be preferred over the result for ideal fluids in low Reynold's number motions. Since the string tension was not measured directly in the yo-yo motion, it is impossible to compare the actual fluid drag with the predicted value to see if they really were the same. In the case of the off-center bodies, a direct comparison was possible by making a second run, immediately after the first, in which the center of mass was directly below the geometric center. The drag on the rotating bodies appeared to show a systematic increase of about 4 per cent as $Re_{\omega} \equiv \frac{a^2\Omega}{\nu}$ increase from 0 to 0.006 to 0.011; however, the absolute error in this range was at least 10 per cent so that these measurements though interesting, are far from conclusive.

Table 31. Spherical Bodies

Fluid Medium	Type of Motion	Viscosity (cgs)	Re	$\varepsilon^{\circ}_{exp}$	$\varepsilon_{th}/\varepsilon_{exp}$
C.O	yo-yo	7.84	0.148	4°40'	1.04
C.O.	yo-yo	7.86	0.139	4°12'	1.13
C.O.	off-center	7.65	0.132	0° 9'	1.3

Table 32. Cylindrical Bodies

Fluid Medium	Type of Motion	Re	Body Length	ε_{exp}	$\varepsilon_{th}/\varepsilon_{exp}$
W.	yo-yo	0.295	6.38	29'	11.0
W.	off-center	0.846	6.38	14'	8.7
W.	yo-yo	1.293	12.57	1°10'	4.5

The above results are even more inconclusive than those for the sphere. Since no lift relation for low Reynold's numbers is known, the relation given by inviscid theory was used, and no attempt was made to maintain a small value of Reynold's number on the falls. There is a definite trend in the $\epsilon_{th}/\epsilon_{exp}$ values; however, it is not possible to conclude, say, that the indicated decrease in this ratio is strictly due to increasing length of the cylinder as opposed to the Re number associated with the motion. In particular, the rotational rate of the off-center body was an order of magnitude smaller than that of the yo-yo. Due to the small size of the tank containing castor oil, it was impossible to obtain decent results in that medium.

Conclusions

The data discussed above represent only a very small sample of the total. Over 200 such motions were actually photographed. However, as these sample results indicate, the experimental setup was far from ideal, so that, rather than trying to make these measurements more precise, the decision was made to do the work discussed in the main part of this dissertation. I feel that the work discussed here may still have some merit if for no other reason than to indicate some of the pitfalls associated with it to later workers in the field. Also, as a result of these investigations, several alternate approaches to the problem have become apparent. For example, by using a more viscous fluid than whiterex, it should be possible to use larger bodies which have a rotational drive mechanism inside them.

In concluding this section it might be mentioned that a number of other effects were photographed during this period. Quite a few photographs have been taken of the fall of two-sphere configurations whose orientation relative to one another was fixed. In particular, the case of the identical spheres constrained to touch was investigated. For low Reynold's number motion, the orientation of the line of centers of the spheres relative to the vertical, β, should remain fixed as they fall. However, their line of motion should deviate from the vertical as a function of β according to the relation

$$\tan \varepsilon = \frac{0.099 \tan \beta}{1 + (0.901)\tan^2\beta} , \qquad (55)$$

which has $\varepsilon = 0$ at $\beta = 0, \pi/2$ as would be expected, and gives $\varepsilon_{max} = 2°59'$ at $\beta_{max} = 46°29'$.[49] The photographic data, on the other hand, appeared to show $\varepsilon_{max} \simeq 5°$ at $\beta \simeq 52°$. However, the spheres used were, again, of poor quality, and were not quite identical. Now that high quality spheres are available and a better experimental set-up has been arranged, it should be possible to check this theory with much higher precision.

BIBLIOGRAPHY

1. Newton, Sir Isaac, Principia, Book 2, Prop. 32, "On the Attrition of Liquids".
2. Navier, C.L.M.H., "Memoir on the Laws of Motion of Fluids", Mem. Acad. Sci. Paris, 6, 389 (1823).
3. Stokes, Sir G. G., "On the Effect of the Internal Friction of Fluids on the Motion of Pendulums", Trans. Camb. Phil. Soc. 9, Part II, 8 (1851).
4. Whitehead, A. N., "Second Approximation to Viscous Fluid Motion", Quart. J. Math. 23, 78 (1889).
5. Oseen, C. W., "Uber die Stokes' sche Formel, und über eine verwandte Aufgabe in der Hydrodynamik", Arkiv. Math. Astron. Fysik, 6, #29 (1910).
6. Kaplun, S. and Lagerstrom, P. A., "Asymptotic Expansions of the Navier-Stokes Solutions for Small Reynold's Numbers", J. Math. Mech. 6, #5, 585 (1957).
7. Van Dyke, Milton, Perturbation Methods in Fluid Mechanics, Academic Press (1964).
8. Kaplun, Saul, Fluid Mechanics and Singular Perturbation Problems, edited by P. A. Lagerstrom, L. N. Howard, Ching-shi Lui, Academic Press (1968).

9. Proudman, I. and Pearson, J.R.A., J. Fluid Mech. 2, 237 (1957).

10. Lagerstrom, P. A. and Cole, J. D., "Examples Illustrating Expansion Procedures for the Navier-Stokes Equations", J. Rat. Mech. Anal. 4, 817 (1955).

11. Chang, I. D., "Navier-Stokes Solution at Large Distances from a Finite Body", J. Math. Mech. 10, 811 (1961).

12. Happel, J. and Pfeffer, R., "On the Motion of Two Spheres in a Viscous Fluid", A. I. Ch. E. Jour. 6, 129 (1960).

13. Maxworthy, T., "Accurate Measurements of Sphere Drag at Low Reynold's Numbers", J. Fluid Mech. 23, 369 (1965).

14. Chemical Engineering Handbook, 3rd edition, J. Perry (ed.), (1950).

15. Broersma, S., "Viscous Force on a Moving Sphere", Bull. Am. Phys. Soc. 10, 167 (1965); W. H. Dodson, "The Motion of Cylinders and Disks in a Viscous Medium", (University of Oklahoma, M.S. Thesis, 1963).

16. Carrier, G. F., "On Slow Viscous Flow", Final Report, Office of Naval Research (1953).

17. Ladenburg, R., "On the Influence of Walls on the Motion of a Sphere in a Viscous Fluid", Annals of Physics 23, 447 (1907).

18. Faxén, H., Arkiv. Mat. Astron. Fys. 17, #27 (1923).

19. Bohlin, T., Trans. Roy. Inst. Tech., #155 (1960).

20. Haberman, W. L. and Sayre, R. M., "David Taylor Model Basin, Report #1143", U. S. Department of the Navy (1953).

21. Lorentz, Abhandlungen über Theoretische Physik, Lepzig (1907).

22. Barr, G., A Monograph of Viscometry, p. 184, Oxford University Press (1931).

23. Tanner, R. I., "End Effects in Falling-Ball Viscometry", J. Fluid Mech. 17, 161 (1963).

24. Tucker, W. H. and Broersma, S., "Force on a Stationary Sphere", Phys. Fluids, 7, 1864 (1964); Bull. Am. Phys. Soc. 8, 498 (1963).

25. Happel, J. and Brenner, H., Low Reynold's Number Hydrodynamics, Prentice-Hall, (1965).

26. *Loc. Cite,* 22.

27. Hugel (ed.), Liquids: Structure, Properties, and Solid Interactions, Elsevier, 226 (1965).

28. Castleman, R. A., "The Resistance to the Steady Motion of Small Spheres in Fluids", Nat. Adv. Comm. Aero., Tech. Note # 231 (1926).

29. Broersma, S., Bull. Am. Phys. Soc. 10, 167 (1965).

30. *Loc. Cite,* 16.

31. Lamb, Sir Horace, Hydrodynamics, 6th edition (1932), p. 594.

32. *Loc. Cite,* 25, p. 298.

33. *Ibid,* p. 235.

34. *Ibid,* p. 85.

35. Langlois, Slow Viscous Flow, p. 136 (1964).

36. *Loc. Cite,* 25, p. 267.

37. *Ibid,* p. 327.

38. *Ibid,* p. 318.

39. Tait, P. G., Trans. Roy. Soc. Edinburg, 37 and 39.

40. *Ibid.*

41. *Ibid.*

42. *Ibid.*

43. *Ibid.*

44. Proudman, I. Proc. Roy. Soc. London A, (1916).

45. Taylor, Proc. Roy. Soc. London A, (1917).

46. Garstang, Proc. Roy. Soc. London A, 142 (1943) 491.

47. Rubinow and Keller, Journal of Fluid Mechanics, 1961.

48. *Loc. Cite,* #15.

49. *Loc. Cite,* #25.